[AMERICAN JOURNAL OF SCIENCE, VOL. 284, JUNE, 1984, P. 597-650]

American Journal of Science

JUNE 1984

CONTACT SKARN FORMATION AT ELKHORN, MONTANA. I: P-T-COMPONENT ACTIVITY CONDITIONS OF EARLY SKARN FORMATION*

JOHN R. BOWMAN** and ERIC J. ESSENE

Department of Geology and Mineralogy,
The University of Michigan, Ann Arbor, Michigan 48109

ABSTRACT. Mineralogically zoned magnesian skarns are extensively developed in at least four time stages in dolomitic marbles on the upper sides and top of the Black Butte Stock near Elkhorn, Mont. The initial stage of skarn development (I) is characterized by a variety of three-phase and less often four-phase assemblages which usually include garnet and pyroxene and occasionally epidote, vesuvianite, or clintonite. Three major zonation types — Massive, Contact, and Nodule — can be distinguished on the basis of zonation scale and mineralogical sequence in the dominant primary stage I skarns. Mineral zones within the Massive skarns are imperfectly zoned with respect to the contact with the Black Butte Stock. The second stage of skarn development (II) was marked by local replacement of garnet and pyroxene upon cooling by one or more of epidote, amphibole, clintonite, chlorite, calcite, and quartz. Limited quartz–axinite veining and chloritization of pyroxene-rich skarns constitute stages III and IV, respectively.

Electron microprobe analyses indicate wide variations in pyroxene (Di_{40-96}, Hd_{0-60}, $AlTs_{0-42}$, $FeTs_{0-22}$) and garnet (Ad_{5-78}, HGr_{0-14}, Gr_{22-95}) compositions in stage I. However, mineral grains on a thin section scale are seldom extensively zoned (for example, in excess of 5 mole percent). Neither phase composition is completely buffered by mineral assemblages, nor are phase compositions simple functions of location within the skarns or zonation type. These compositional variations, even within nominally buffered assemblages, record variations in intensive chemical parameters such as $a(SiO_2)$, $a(FeO_x)$, $X(CO_2)$, $a(Fe_2O_3/Al_2O_3)$ (for garnets), and possibly $f(O_2)$.

Application of experimental and calculated phase equilibria to observed skarn assemblages has allowed estimations of general physical-chemical conditions of formation for stage I skarns: $P = 1.0 \pm 0.3$ kb, $T = 525 \pm 35°C$, $0.04 < X(CO_2) < 0.30$, $-22.7 < \log f(O_2) < -19.0$, $\log f(S_2) < -3.3$, $-1.65 < \log a(SiO_2) < 0.0$, $-1.85 < \log a(Al_2O_3) < +0.1$. The hydration and carbonation reactions that characterize stage II occurred at lower temperature ($T \leqslant 470°C$) and in a water-rich fluid [$0.05 < X(CO_2) < 0.15$].

* Contribution 351 from the Mineralogical Laboratory, The University of Michigan, Ann Arbor, Michigan 48109

** Current address: Department of Geology and Geophysics, University of Utah, Salt Lake City, Utah 84112

The mineralogic and chemical complexity of the Elkhorn skarns indicates that metasomatism and zone formation cannot be attributed to any simple diffusion and/or infiltration model involving gradients of only one compositional variable. In fact detailed definition of compositional variables within any one zone or of those responsible for mineral zonation and zone-boundary reactions is often precluded by lack of low-variance assemblages. If skarn formation was an isothermal/isobaric process, variations in mineralogy and mineral compositions do indicate at least local gradients in $X(CO_2)$, $a(SiO_2)$, $a(Al_2O_3)$, and probably $a(FeO_x)$. Variations in $f(O_2)$ are suggested by variations in iron partitioning between garnet and pyroxene, but overlapping $f(O_2)$ limits determined for skarn zones, pluton, and pre-existing marble could allow skarn formation at essentially constant $f(O_2)$.

Phase equilibria applications indicate the entire zoning sequence of the Massive skarns could have equilibrated within a continuous gradient in $X(CO_2)$ from 0.30 ± 0.05 at the skarn-marble interface to 0.03 to 0.07 at the intrusive contact. Estimates of mass-transfer of chemical components, measured variations in mineral compositions, and the large chemical potential differences for CO_2 between the marble and intrusion are consistent with such gradients in $X(CO_2)$.

NOTATION

ΔG_f^o = standard state free energy of formation (298 K, 1 bar)
S_i^o = standard state entropy of phase i (298 K, 1 bar)
ΔH_R = enthalpy change of reaction (T, 1 bar)
P_T = lithostatic pressure (bars)
P_f = fluid pressure (bars)
T = temperature (°C unless otherwise indicated)
$X(CO_2)$ = $pCO_2/(pCO_2 + pH_2O)$, assuming ideal mixing of CO_2 and H_2O
X_i^j = mole fraction of component i in phase j
p_i = partial pressure of component i
a_i^j = activity of component i in phase j
f_i^j = fugacity of component i in phase j
μ_i^j = chemical potential of component i in phase j
K = equilibrium constant
R = gas constant

MINERAL ABBREVIATIONS

Ad = andradite garnet
Amp = amphibole
And = andalusite
Ak = ackermanite
An = anorthite
Ap = apatite
Ax = axinite
Bi = biotite
Br = brucite
Cc = calcite
Cp = chalcopyrite
Chl = chlorite
Clt = clintonite
Di = diopsidic pyroxene
Ep = epidote
Fo = forsterite
Gr = grossular garnet
Gn = grandite garnet

Kfs	= potassium feldspar	Qz	= quartz
Mo	= monticellite	Ru	= rutile
Mt	= magnetite	Sc	= scapolite
Pe	= periclase	Sp	= spinel
Pg	= plagioclase	Sph	= sphene
Po	= pyrrhotite	Srp	= serpentine
Pr	= perovskite	Tr	= tremolite
Px	= pyroxene	Vs	= vesuvianite
Py	= pyrite	Wo	= wollastonite

INTRODUCTION

Comparatively few integrated stable isotope-petrologic studies have been conducted on contact skarn deposits adjacent to shallow plutons despite their economic and petrologic importance. Several recent studies have focused on some aspects of skarn zoning, mineral compositions, and paragenesis (Einaudi, 1977; Kerrick, 1977; Kwak, 1978a; Collins, 1977; Einaudi and Burt, 1982) or on the general conditions of skarn formation (Morgan, 1975; Kerrick, 1977; Taylor and O'Neil, 1977; Kwak, 1978b). All these studies have dealt with the Fe-rich calcic skarns associated with tungsten or copper mineralization. Comparatively few studies (Kerrick, 1977; Shedlock and Essene, 1979) have dealt with the SiO_2-undersaturated magnesian skarns typically formed in dolomitic marbles. Because of the typically high variance of skarn assemblages, petrologic studies alone usually have not been able to define close limits to chemical variables ($f(O_2)$, $X(CO_2)$, et cetera) or the roles of these variables in skarn zonation and petrogenesis. With one exception (Taylor and O'Neil, 1977) little attention has been given to the origin and chemical evolution of skarn fluids.

Carefully integrated stable isotope and petrologic studies may provide detailed information on the physical-chemical variables involved in skarn petrogenesis not derivable from restricted studies using petrology or isotopes alone. We have, therefore, conducted an integrated petrologic-stable isotopic analysis of the zoned skarns and associated rocks in the contact aureole of the Black Butte stock near Elkhorn, Mont. The zonation, paragenesis, mineralogy, and mineral compositions of these skarns and of the physical-chemical conditions of their formation are described in part I (this paper). The stable isotope results dealing with fluid sources, mass transfer, and evolution of fluid compositions are presented in part 2.

GENERAL GEOLOGY

Several small gabbro/quartz–diorite stocks representing early mafic phases of the nearby Boulder Batholith intrude and metamorphose a late Precambrian to Paleozoic sequence of dolomite with mudstone and minor calc-pelite at Elkhorn, Mont. (Klepper, Weeks, and Ruppel, 1957). The dolomitic marbles have been extensively replaced by garnet–pyroxene skarns at the intrusive contact of the Black Butte stock (fig. 1). Skarns are more extensively developed on the upper sides and top of the intrusion

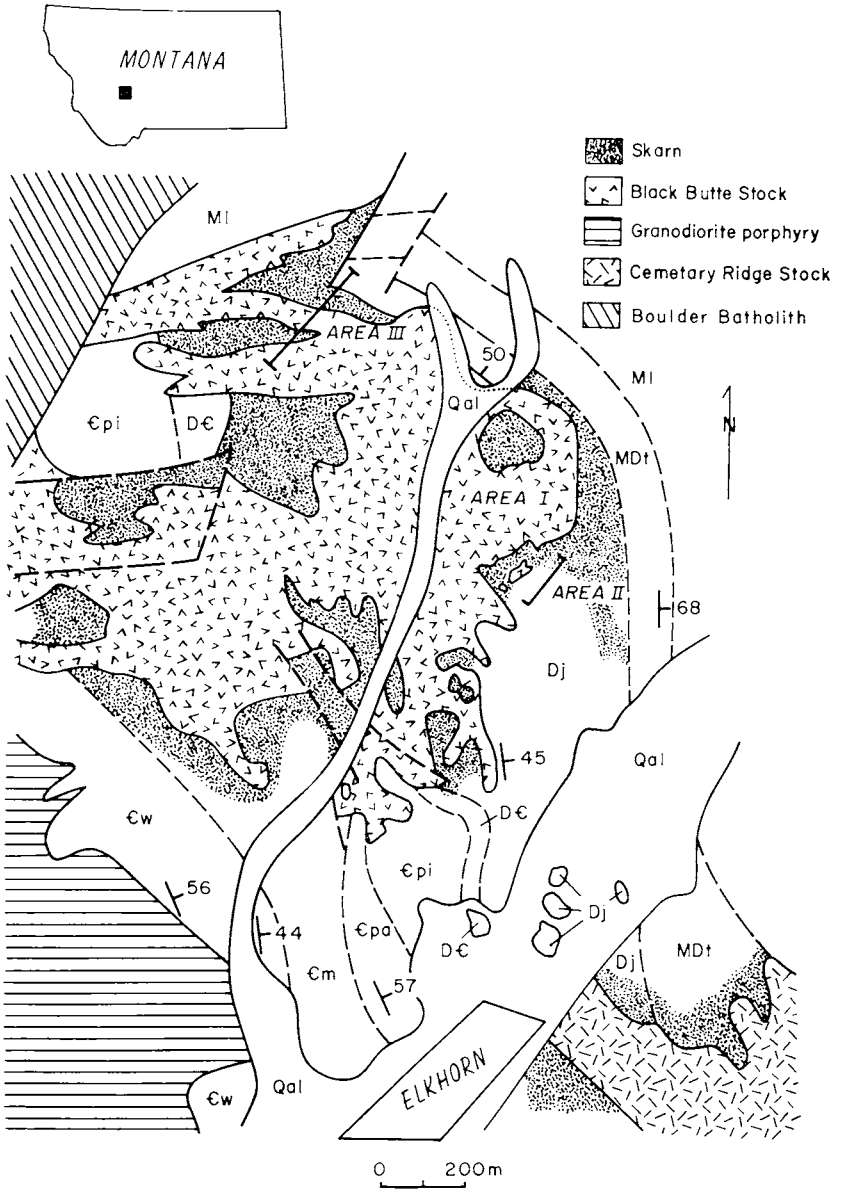

Fig. 1. Geologic map of the Black Butte contact aureole (modified from Klepper, Weeks, and Ruppel, 1957) illustrating geologic relations between the Black Butte quartz-diorite, contact replacement skarns and surrounding country rock. Most of the country rock is carbonate (dolomite), with the exceptions of the Park (€pa), Wolsey (€w), and Three Forks (MDT) shales. Other formation abbreviations are €m = Meagher limestone, €pi = Pilgrim dolomite, D€ = Red Lion formation, Dj = Jefferson dolomite, Ml = Lodgepole limestone, Qal = alluvium. Areas I to III are discussed in the text. Heavy lines are faults, dashed where approximately located. The Black Butte stock is irregular in outcrop geometry, displaying numerous reentrants and several roof pendents of variable size. These localities are sites for extensive development of massive garnet–pyroxene skarns. The attitude of the igneous contact can fluctuate from nearly vertical to sub-horizontal over small distances. Skarn is developed at the igneous contact to a maximum of about 120 m below the elevation of the highest preserved skarn. These features suggest that present exposures are in the uppermost parts of the intrusion.

(for example, the roof pendant labeled area I), within marble reentrants at geometric irregularities in the intrusive contact, or immediately below impermeable shale units (Klepper, Weeks, and Ruppel, 1957; Bowman, ms). Along several sections of the southeastern intrusive contact, the skarn is usually either thin (< 20 cm) or absent. These portions of the igneous contact are geometrically regular and at structurally lower levels, approx 120 m or more below the highest preserved skarn (areas I and III). These geologic relations suggest dominant upward and outward flow of the skarn fluids from the upper parts of the intrusion and along the intrusion/wallrock contact. The skarns are variable in thickness from a few centimeters up to 25 to 30 m, where exposures are sufficient for accurate measurement. Apparent skarn thicknesses exceeding 80 to 150 m have been mapped along the south and northeast segments of the contact, but poor exposures in these areas prevent determination of accurate thickness or the nature of the intrusive contact. In one of these areas (northeast contact) nearby contact metamorphosed marble containing forsterite and calcite indicates the possibility of igneous rock at shallow depth (Bowman and Essene, 1982). Therefore actual skarn thickness in this area may be considerably less.

SKARN PETROLOGY, PARAGENESIS, AND ZONATION

The contact skarns were formed in four stages (table 1). Stage I was volumetrically the most important and consisted of the replacement of homogeneous dolomitic marble by massive skarn dominated by garnet and pyroxene. Stage II was marked by the local replacement of garnet and pyroxene by combinations of epidote, amphibole, biotite, clintonite, chlorite, calcite, and quartz. Stage III consisted of the minor development of axinite-bearing quartz veins with epidote, chlorite, and calcite. Stage IV consisted of fracturing and shearing of earlier formed skarn with replacement by chlorite and serpentine along these shear zones. Locally the degree of shearing and replacement was extensive. In the following sections, the first two stages will be more thoroughly discussed.

Stage I

The dominant skarn assemblage of this stage consists of grandite garnet plus diopsidic pyroxene (with variable and often significant amounts of tschermaks and hedenbergite components), often with minor calcite and accessory sphene, apatite, and, less commonly, magnetite (pl. 1-A, -B). Textural evidence indicates pyroxene formed prior to and with garnet. Inclusions of magnetite in both pyroxene and garnet (pl. 1-A) indicate that the magnetite crystallized prior to and with pyroxene and prior to garnet. Textural relations indicate calcite formed before and with garnet and pyroxene (pl. 1-B). However, some calcite continued to crystallize after garnet and pyroxene, as it also occupies pore spaces interstitial to these phases. The stage I skarns are mineralogically variable (table 1) and unusual in that they contain vesuvianite, epidote, and clintonite associated with, but not replacing, garnet and pyroxene. These occurrences contrast sharply with the more typical replacement mode of occurrence

TABLE 1

Stage	General Characteristics
I	The initial stage of development of magnesian skarn by massive replacement of low SiO_2 and Al_2O_3 dolomitic marble at or near the intrusive contact of the Black Butte Stock. This stage constitutes $\geq$ 90 percent by volume of exposed skarn and involves extensive mass transfer of SiO_2, Al_2O_3, FeO_x, and CO_2 at volume changes = 0 $\pm$ 20 percent, based on observed stratigraphic and porosity variations. This stage is characterized by mineralogical zonation on several scales, defining three major skarn types (see table 2 and text): MASSIVE CONTACT NODULE
II	The local and usually partial replacement of stage I assemblages or minerals by hydrous silicates $\pm$ Cc, Qz, Mt, and/or Py. The common replacement relationships are detailed in the next column. Accompanying volume changes are often indeterminate, but psuedomorphous replacement ($\Delta V \approx 0$) is not rare. Replacement reactions probably occur over a range of T-a(fluids) conditions.
III	Minor development of cross-cutting axinite (Ax)-bearing veins. Volume changes are indeterminate.
IV	Extensive serpentinization and/or chloritization of post-skarn shear zones. Volume changes are indeterminate.

that characterizes these hydrous silicates in the later stages of skarn development at Elkhorn and in most skarns.

Epidote exhibits contemporaneous textural relationships with pyroxene and scapolite (pl. 1-C). Textural relations (pl. 1-D) indicate that vesuvianite formed after pyroxene but before garnet. Both assemblages are restricted to the inner part of the skarns closest to the intrusion. All occurrences of texturally primary epidote occur very near the igneous contact (within 50 cm), whereas vesuvianite-bearing rocks extend to a maximum of about 50 m away from the nearest exposed igneous contact (along the northeast and southern sections of the igneous contact, fig. 1).

Clintonite assigned to stage I does not replace or react with adjacent pyroxene, garnet, or spinel (pl. 1-E and -F), nor is it restricted to fractures or veinlets within mineral grains or open-space vugs or voids between garnet and pyroxene crystals. Clintonites of this type are associated with *Gn* + *Px* + *Vs*, *Gn* + *Px* $\pm$ *Cc* and *Gn* + *Px* + *Sp* + *Cc* (pl. 1-E and -F) assemblages, which are restricted to the inner and intermediate portions

TABLE 1 (continued)

Mineralogy

The typical skarn assemblage consists of grossular-andradite garnets and compositionally complex Ca-pyroxene with one or more of the minor phases calcite, sphene, and magnetite. However, the skarns in total are characterized by a variety of three- and four- phase assemblages, of which the most important are (in approximate order of abundance): Gn + Px + Cc; Gn + Vs + Px + Cc; Px + Clt + Sp; Px + Sp + Cc; Gn + Px + Pg; Gn + Px + Clt + Cc; Gn + Px + Sp + Cc; Px + Ep + Sc + Cc; and Px + Pg + Cc. In addition, there are several other uncommon, but petrogenetically significant, assemblages which are discussed in the text. Additional phases, which occur sporadically, are quartz, wollastonite, forsterite, perovskite, pyrite, and chalcopyrite.

Amp + Cc + Qz after Px
Amp or Chl + Cc after Gn
Ep after Pg and Gn
Ep + Qz + Cc + Py after Gn
Clt + Chl after Px + Sp
Clt after Gn
Bi after Px

Ax + Ep + Chl + Qz + Cc
Ax + Ep
Ep + Chl + Amp + Qz + Cc

Serpentine (Srp) + Chl after Px and Gn

of the Massive skarns (figs. 1 and 2), with respect to the igneous contact, and *Px + Sp + Cc* assemblages in the outer portions of the skarn. Grain-boundary contacts between subhedral clintonite assigned to stage I and pyroxene and garnet appear contemporaneous, but clintonite inclusions are not observed in either garnet or pyroxene, whereas clintonite sometimes contains included pyroxene. Therefore clintonite probably started to crystallize after pyroxene, and perhaps garnet, started to crystallize. An exception may be the Nodule skarns (see below), where clintonite and garnet appear to be contemporaneous (pl. 2-A).

Although textural evidence is not always definitive, it generally supports the existence in many samples of three (and occasionally more) near-contemporaneous mineral assemblages. Some observations, also included in plates 1 through 3 do suggest some differences in the timing of crystallization of garnet, pyroxene, vesuvianite, calcite, and clintonite but without reaction relationships between minerals. The sequence inferred above for these minerals is based on observations that certain minerals

PLATE I

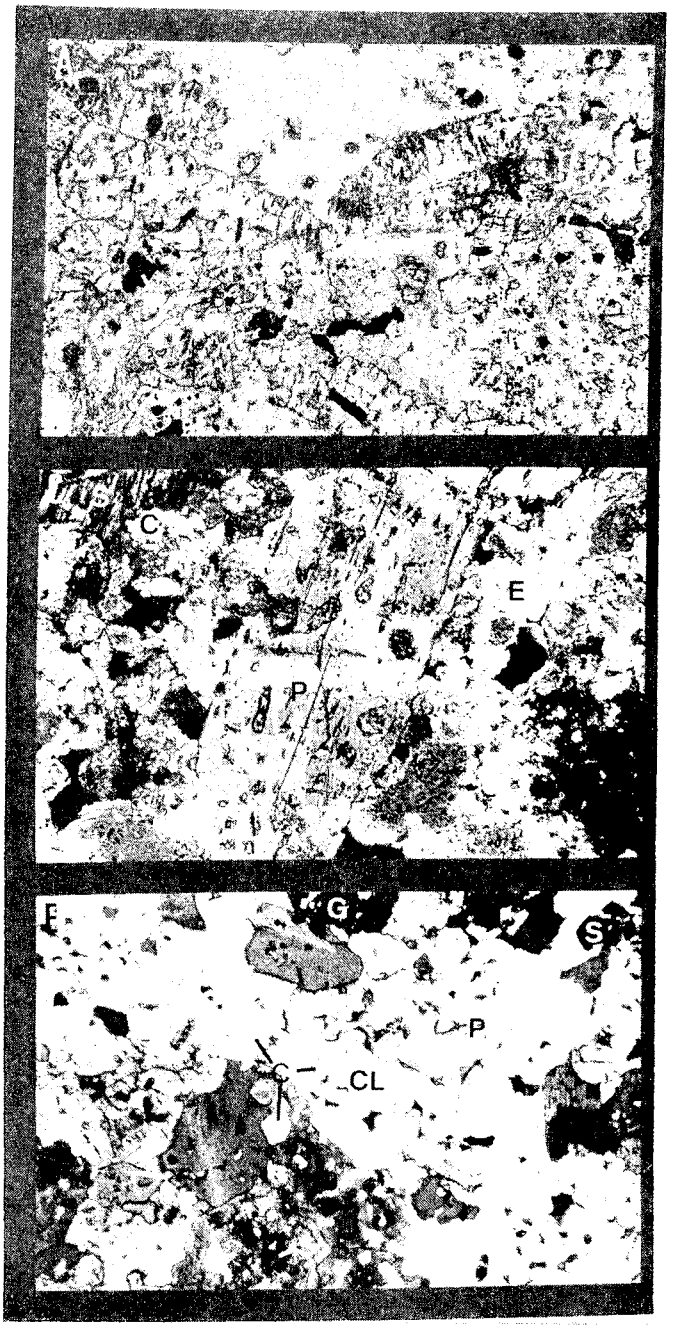

A. Photomicrograph showing magnetite (M) inclusions in pyroxene (P) and garnet (G). Stage I, Massive skarn. Plane light. × 6.3.

C. Photomicrograph of the Contact skarn assemblage pyroxene (P), epidote (E), scapolite (S), and calcite (C). Crossed nicols. × 16.

E. Photomicrograph of the stage I assemblage garnet (G), pyroxene (P), clintonite (CL), spinel (S), and calcite (C). Crossed nicols. × 6.3.

PLATE 1 (continued)

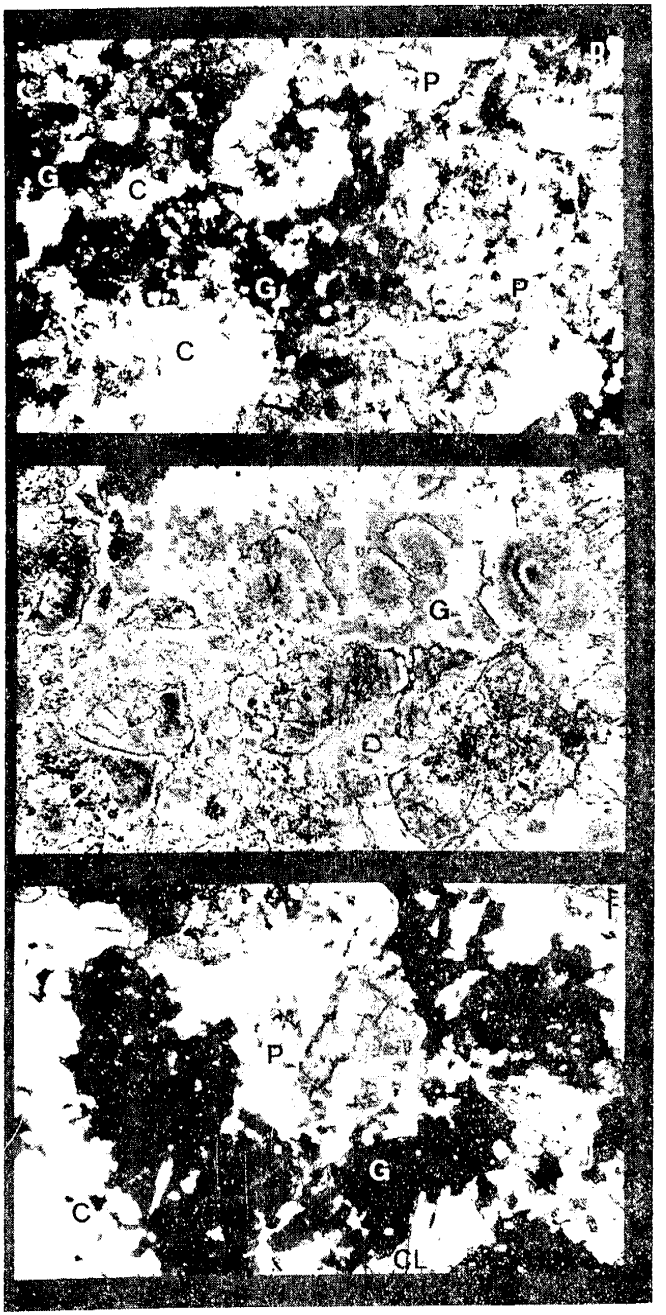

B. Photomicrograph showing the stage I assemblage garnet (G), pyroxene (P), and calcite (C). Crossed nicols. × 6.3.

D. Photomicrograph of the stage I skarn assemblage pyroxene (P), vesuvianite (V), and garnet (G) in the Massive skarn. Plane light. × 6.3.

F. Photomicrograph of the stage I assemblage garnet (G), pyroxene (P), clintonite (CL), and calcite (C). Crossed nicols. × 6.3.

appear to "wrap-around" or include others, while the reverse is not observed. Minerals are assigned to stage I when they are not found in voids, veins, or fractures and where they are closely associated without evidence of replacement. It will be assumed, for the purposes of this paper, that the minerals assigned to stage I are at minimum broadly contemporaneous and are in a state of equilibrium. Textural evidence supporting this assumption has been provided in the accompanying photomicrographs. While others might infer from these textures some degree of disequilibrium, we interpret these textures to indicate a reasonable approach to equilibrium for certain key mineral assemblages. In the fol-

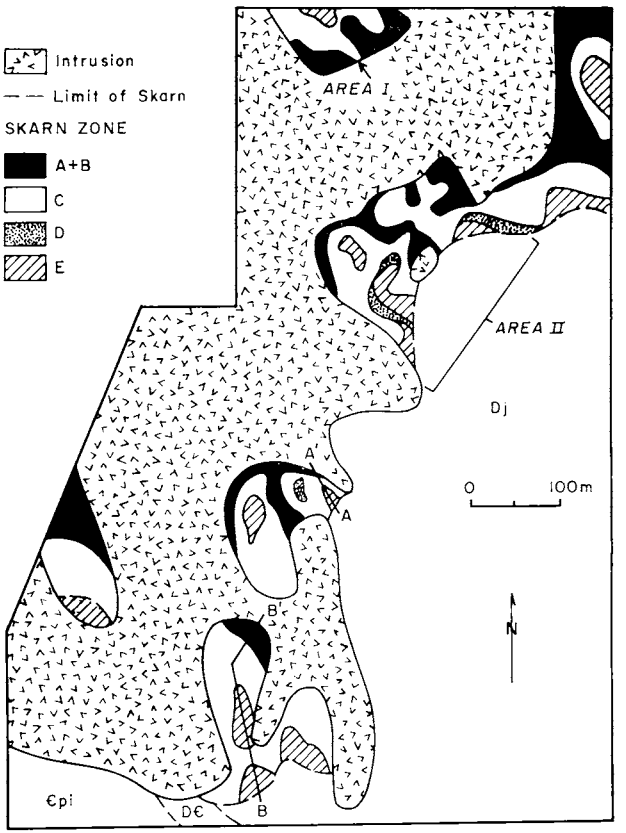

Fig. 2. Geologic map of the eastern portion of the Black Butte aureole, summarizing the distribution of the predominant mineral zones of the Massive skarns (see table 2). The mineral zones plotted in any area are the dominant mineralogies of the skarns. Fine-scale variations in mineralogy and irregularities in zone boundaries have not been plotted to emphasize general skarn zonation patterns. The letters designate each mineral zone as defined in the text: A = *Px* + *Ep* + *Sc* + *Cc*; B = *Gn* + *Px* + *Vs* ± *Cc*; C = *Gn* + *Px* + *Cc*, absence of *Vs* and *Sp*; D = *Gn* + *Px* + *Pg* ± *Cc* or *Gn* + *Px* + *Sp* ± *Clt* ± *Cc*; E = *Px* or *Px* + *Sp* + *Cc* or *Px* + *Pg* ± *Cc*, absence of *Gn* and *Vs*. Detailed sampling was conducted in areas I, II, and III (fig. 1) and along traverses A-A′ and B-B′.

lowing sections, this interpretation will be utilized to place limits to some compositional variables for various skarn assemblages. This will hold especially for *Clt*-, *Vs*-, and *Cc*-bearing assemblages, and the limits should be considered in light of this assumption.

This interpretation of equilibrium is supported indirectly by several textural characteristics of the skarns. The mode of occurrence of the hydrous silicates and calcite assigned to stage I are in marked contrast to those marking the stage II of skarn development at Elkhorn and in many other skarns. In stage II at Elkhorn, epidote, clintonite, amphibole, and calcite clearly cross-cut and replace earlier formed garnet and/or pyroxene or are restricted to obvious void-filling. With regard to the abundance and mode of occurrence of hydrous silicates, stage I of the Elkhorn skarns is unusual with respect to many skarns. The absence of reaction relationships is particularly significant for phases such as clintonite and vesuvianite. For example, topological analysis of phase equilibria involving *Gn*, *Px*, *Sp*, *Clt*, and *Cc* (Bowman, ms; Bowman and Essene, 1979) indicates that the anhydrous phases plus calcite are reaction products of stable, clintonite-bearing reactions. Preliminary calculations indicate these reactions to be stable at the P-T-X(CO_2) conditions estimated for stage I (see later discussion). A similar situation holds for vesuvianite (Valley and others, ms). It will be shown in a later section that pyroxene and clintonite have a very restricted range of composition in the uncommon *Gn* + *Px* + *Clt* + *Sp* + *Cc* assemblages, relative to the total compositional variation observed. In addition, both pyroxene and clintonite compositions correlate with the mineralogy of definitive mineral assemblages. These compositional characteristics are also consistent with the interpretation of equilibrium.

Stage I Zonation

Petrologically, the stage I skarns are spatially heterogeneous or zoned on several scales. Based on the scale of zonation and position within the skarns, three distinct types of mineralogically zoned skarns can be defined (table 2): Contact, Massive, and Nodule skarns.

Contact skarns.—Contact skarns are those skarns that formed at the igneous contact and that are zoned mineralogically on a small scale ($\leqslant$ 8-12 cm). All contain a thin (2-40 cm) anhydrous *Px* + *Pg* + *Sph* ± minor *Qz* "endoskarn" developed within the intrusion. Two zonation sequences have been observed (table 2). The usual sequence away from the stock is: endoskarn → *Gn* + minor *Px* → *Px* + minor *Gn* → *Px* + *Sp* ± minor *Gn* (pl. 2-B). The last zone is not always present. Some sequences contain a *Gn* + *Pg* zone adjacent to the endoskarn. A less common sequence in area I (fig. 2), but one found more often in area II and along the northwest border of the Black Butte stock, is from the igneous contact outward: endoskarn → *Px* + *Ep* + *Sc* + *Cc* → *Px* + *Sc* + *Cc* → *Px* + *Sc* + *Gn* + *Cc* → Massive *Gn* + *Px* ± *Vs* skarn. Although *Ep* and *Gn* are found within the same thin section because of the scale of this zonation, they are not in contact and are separated by a zone of *Px* + *Sc*. Individual zone

PLATE 2

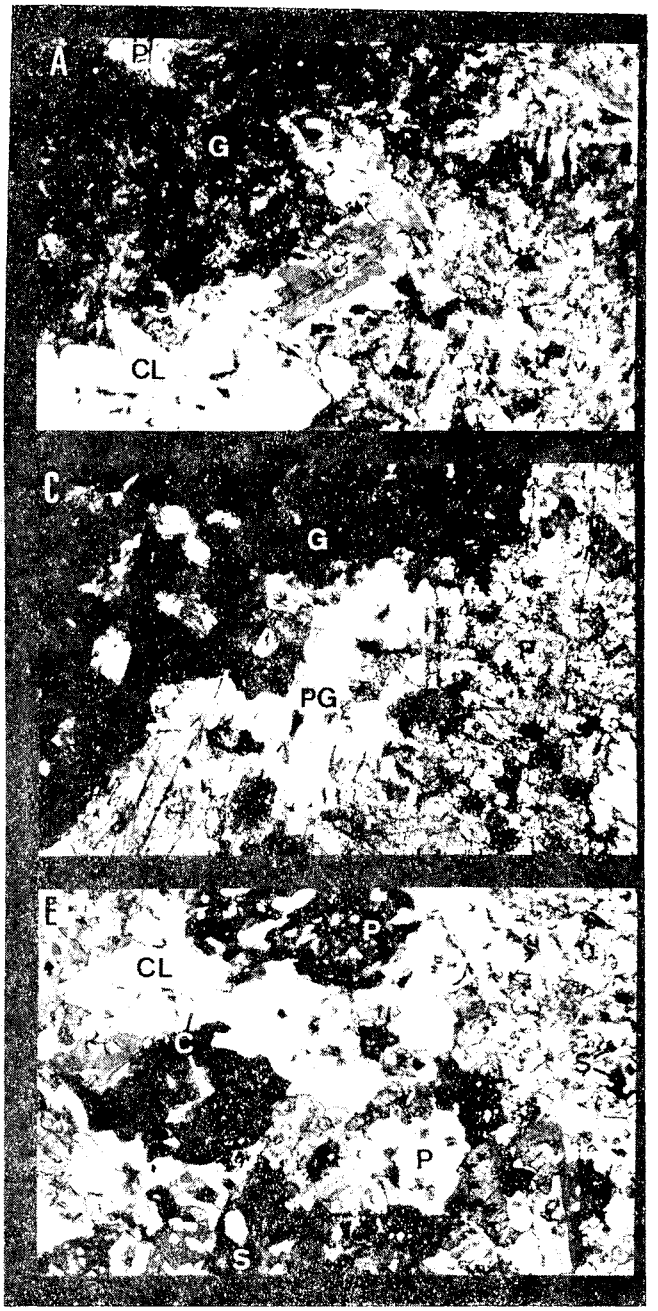

A. Photomicrograph of the Nodule skarn contact between massive clintonite (CL) to the lower right and garnet (G) with included pyroxene (P) and vesuvianite (not shown). Crossed nicols. × 16.

C. Photomicrograph of the stage I assemblage garnet (G), pyroxene (P), and calcium plagioclase (Pg). Massive skarn. Crossed nicols. × 2.5.

E. Photomicrograph of the stage I assemblage pyroxene (P), clintonite (CL), spinel (S), and calcite (C). Calcite inclusions in the pyroxene at extinction (top center) form several optically continuous grains which are not in optical continuity with the adjacent calcite grain to the lower left. Massive skarn. Crossed nicols. × 6.3.

PLATE 2 (continued)

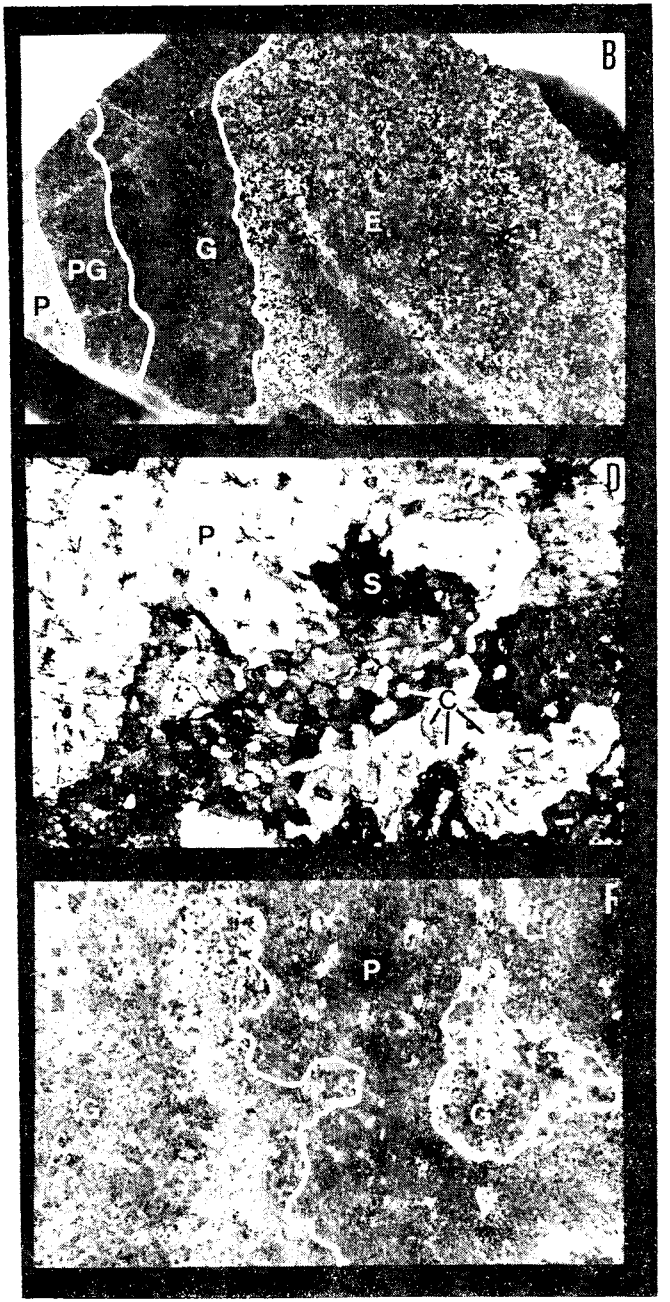

B. This polished slab (8 cm long dimension) is a representative sample of the zoned Contact skarn with zoning starting at the right from Endoskarn (E) — the *Px* + *Pg* + *Sph* zone — to Garnet zone (G) with minor pyroxene to Pyroxene zone (PG) with minor garnet to Pyroxene or Pyroxene plus Spinel zone (P).

D. Photomicrograph of the stage I assemblage pyroxene (P), spinel (S), and calcite (C). Massive skarn. Crossed nicols. × 6.3.

F. Photograph of a thin section (40 mm length) showing the replacement type of zone boundary, in which an abrupt appearance of garnet, without evidence of fracture-filling, marks the *Gn* + *Px* + *Pg*/*Px* + *Pg* boundary. The slide cuts through an irregular boundary, resulting in the apparent isolated pods of *Gn* + *Px* + *Pg* to the right of the slide. Abbreviations are: G = *Gn* + *Px* + *Pg* zone; P = *Px* + *Pg* zone.

PLATE 3

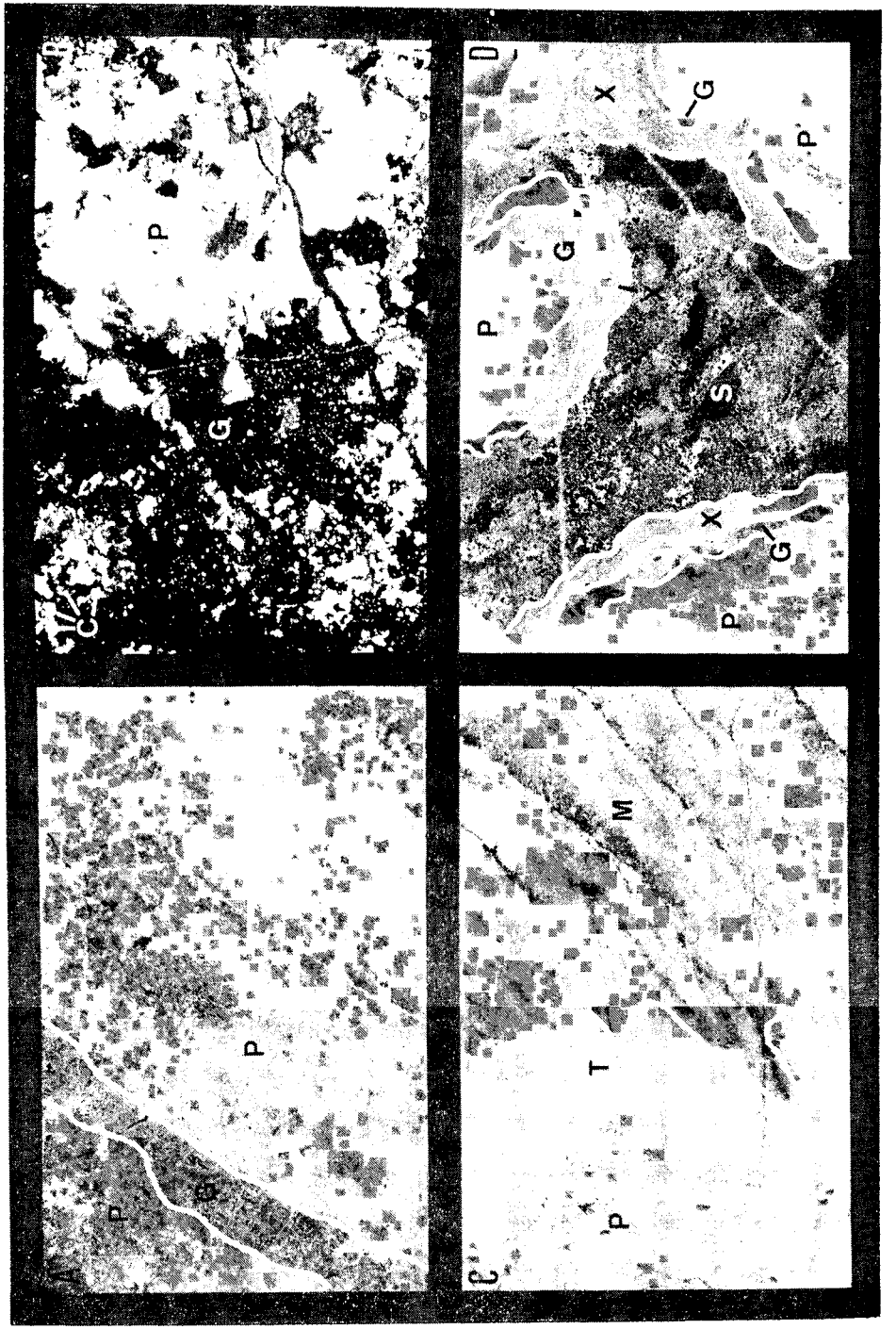

boundaries are sharp and without obvious replacement or cross-cutting relationships. The Contact skarns grade, without obvious replacement relationships, into Massive skarn, either *Gn* + *Px* or *Gn* + *Px* + *Vs*, or rarely into marble.

Massive skarns.—The Massive skarns constitute virtually all the exposed skarn masses in the Black Butte aureole. The mineralogically distinct zones are large scale (2 m to as much as 50 m) and occur in two distinct sequences of zoning (table 2). The less common sequence is best developed and illustrated by the skarns at the east side of the Black Butte stock in area II (figs. 1 and 2). From the intrusive contact outward, the skarns are zoned mineralogically through the sequence: *Gn* + *Px* + *Vs* + *Cc* → *Gn* + *Px* + *Cc* → *Gn* + *Px* + *Pg* → *Px* + *Pg* or *Px* or *Px* + *Sp* + *Cc* → Marble (pls. 1-B, -D, and 2-C, -D). In three samples, fine-grained quartz is found as inclusions in garnet in the inner two zones.

A distinct, more common sequence of mineralogical zonation is developed in several other areas, including area I (figs. 1, 2). Except for the outer garnet-absent zone, skarn mineralogy is typically *Gn* + *Px* + *Cc*. Zonation is actually defined by scattered occurrences of the definitive phases within the massive *Gn* + *Px* skarn. From the intrusive contact outward, the mineralogical sequence is: *Gn* + *Px* + *Vs* ± *Cc* → *Gn* + *Px* ± *Cc* → *Gn* + *Px* + *Sp* ± *Cc* ± *Clt* → *Px* ± *Sp* ± *Clt* ± *Cc* (pls. 1-B, -D, -E and 2-D, -E). In some areas the epidote and scapolite-bearing assemblages of the Contact skarn type replace the vesuvianite-bearing assemblage at the igneous contact or are developed between the igneous contact and *Gn* + *Px* + *Vs* assemblages.

These two sequences of mineral assemblages (table 2) and the epidote-bearing Contact skarns can be usefully grouped into five zones, four of which are sufficiently large to be mappable (fig. 2). In sequence from the igneous contact to the marble-skarn boundary, these zones are defined as:

Zone A:	*Px* + *Ep* ± *Sc* ± *Cc* (Contact skarn)
Zone B:	*Gn* + *Px* + *Vs* ± *Cc*
Zone C:	*Gn* + *Px* + *Cc*; absence of *Vs* and *Sp*

← A. Photograph of a thin section (30 mm length) showing the cross-cutting or fracture-filled type of zone boundary, in which garnet-rich veins or fractures of the *Gn* + *Px* + *Pg* zone (G) cross-cut the adjacent *Px* + *Pg* zone (P). These fractures merge into massive *Gn* + *Px* + *Pg* zone within 1 to 10 cm. This textural relationship implies that the inner *Gn* + *Px* + *Pg* zone grew outward (and upward) at the expense of the *Px* + *Pg* zone.

B. Photomicrograph of the boundary between the *Gn* + *Px* + *Sp* + *Cc* (left) and *Px* + *Sp* + *Cc* (right) zones. Within the garnet "front", several optically continuous, but skeletal pyroxene (P) and calcite (C) grains attest to the massive replacement character of the boundary. Massive skarn. Crossed nicols. × 6.3.

C. Photograph of a polished slab (12 cm in long dimension) which includes the marble/skarn interface. The outer pyroxene zone of the skarn (labeled P) is separated from dolomitic marble (labeled M) by a narrow (< 2 cm) bleached zone (labeled T). The bleached zone differs mineralogically from the marble by absence of brucite (retrograde product of periclase).

D. This polished slab is a sample of the zoned Nodule skarns. Outward from the interior, zonation sequence in this sample is: *Sp* + *Clt*(S), *Clt* + minor *Chl*(X), *Gn*(G), and *Gn* + *Px* + *Vs*(P). Core zones of larger module skarns often contain calcite and rarely forsterite. Zone boundaries are sharp and discontinuous (no gradational contacts) and lack obvious microfracture filling.

TABLE 2

Skarn Type		Zonation sequences (listed in order of abundance)
MASSIVE	I:	Marble → Px + Pg or Px or Px + Sp + Cc → Gn + Px + Pg → Gn + Px + Cc → Gn + Px + Vs + Cc → Intrusion
	II:	Marble → Px + Sp ± Clt ± Cc → Gn + Px + Sp + Cc ± Clt → Gn + Px + Cc → Gn + Px + Vs ± Cc → Intrusion
CONTACT	I:	Marble → Px + Sp ± Gn (rare) → Px + Gn ± Sph → Gn + Px + Sph (exoskarn/endoskarn boundary) Px + Pg + Sph ± Qz → (Intrusion)
	II:	Massive Gn + Px + Vs skarn → Gn + Px + Sc + Cc → Px + Sc + Cc → Px + Sc + Ep + Cc (exoskarn/endoskarn boundary) Px + Pg + Sph ± Qz → (Intrusion)
NODULE	I:	(Core) Sp + Cc + Clt ± Fo → Sp + Clt → Clt ± Chl → Gn → Gn + Px + Vs ± Clt
	II:	(Core) Px + Fo → Px + Sp + Fo → Px + Sp → Gn + Px + Sp → Gn + Px

Zone D: $Gn + Px + Pg + Cc$ or $Gn + Px + Sp \pm Clt \pm Cc$

Zone E: Px; $Px + Sp \pm Cc$; $Px + Pg \pm Cc$; absence of Vs and Gn

These zones are distributed as irregular bands sub-parallel to the igneous contact which are best developed on the eastern side of the Black Butte stock (fig. 2). Zone A is discontinuous and too narrow (< 50-100 cm) to be shown separately from zone B at the scale of figure 2. In detail the individual mineral zones fluctuate in thickness, the zone boundaries as inferred by the distribution of mineral assemblages often appear to be irregular surfaces on small-scale, and some zones are absent in specific areas. However, the sequence of zones was always observed to be the same. The relative proportions of individual zones change significantly within the skarns. Zones B and C are more extensively developed along the northeast margin of the Black Butte stock and in the roof pendant in that area (fig. 2, area I). These areas are the highest elevation skarns preserved in the Black Butte aureole. Zones B and C are also developed extensively along the southern contact. Zone E is more extensively developed along the northwest sector of the igneous contact.

TABLE 2 (continued)

	Comments
	This skarn type is the dominant type in the skarns (> 90 percent by volume of present stage I skarns). Individual mineral zones are typically > 1 m in thickness. Total thickness is ≤ 30 m where measureable. Zone boundaries are both massive replacement and cross-cutting (micro-fracture filling) in character. Most zones were defined on the basis of the presence or absence of a particular mineral assemblage, because zone boundaries were not often exposed.
	This skarn type is interpreted to correspond to the paired endoskarn/exoskarn of Khorzinskii (1959) and is confined to ≤ 8cm to either side of the igneous contact. Individual mineral zones are ≤ 2cm in thickness, with total thickness ≤ 12cm. When in contact with MASSIVE skarn, sequences I and II grade into Px + Sp ± Cc and Gn + Px + Vs assemblages, respectively. Zone boundaries are massive replacement in character.
	Nodule skarns constitute pod-like masses of ≤ 50cm with individual zones of ≤ 15cm. Zone boundaries are massive replacement in character. The outer zone corresponds to the MASSIVE Skarn zone in which they are enclosed.

Contacts between adjacent skarn zones, where exposed, are of several types. Some are sharply gradational (pls. 2-B, -F), with the appearance or disappearance of the definitive mineral of one zone occurring over a very short distance (< 1 cm in most cases) without obvious replacement relationships. Because the skarns are not completely exposed in outcrop, many contacts have simply been defined on the basis of the last of a series of scattered outcrop occurrences of a particular mineral assemblage within massive *Gn* + *Px*, which makes up the bulk of the skarn in these areas (fig. 1, area I, II). Some boundaries are characterized by cross-cutting or replacement relationships (pl. 3-A, -B). These latter features suggest that interior skarn zones may have encroached on adjacent, outer zones by continued micro-fracturing which enabled fluid to flow upward and outward away from the stock contact. However there is no evidence at zone boundaries or within zones of repeated fracturing, filling, or mineral overgrowths as noted in other skarn deposits (Einaudi, 1977; Taylor and O'Neil, 1977). The available evidence from the Elkhorn skarns is consistent with contemporaneous zones and migrating zone boundaries through time, although compelling evidence does not exist to rule out sequential formation of some of the skarn zones. For the following sections, we

PLATE 4

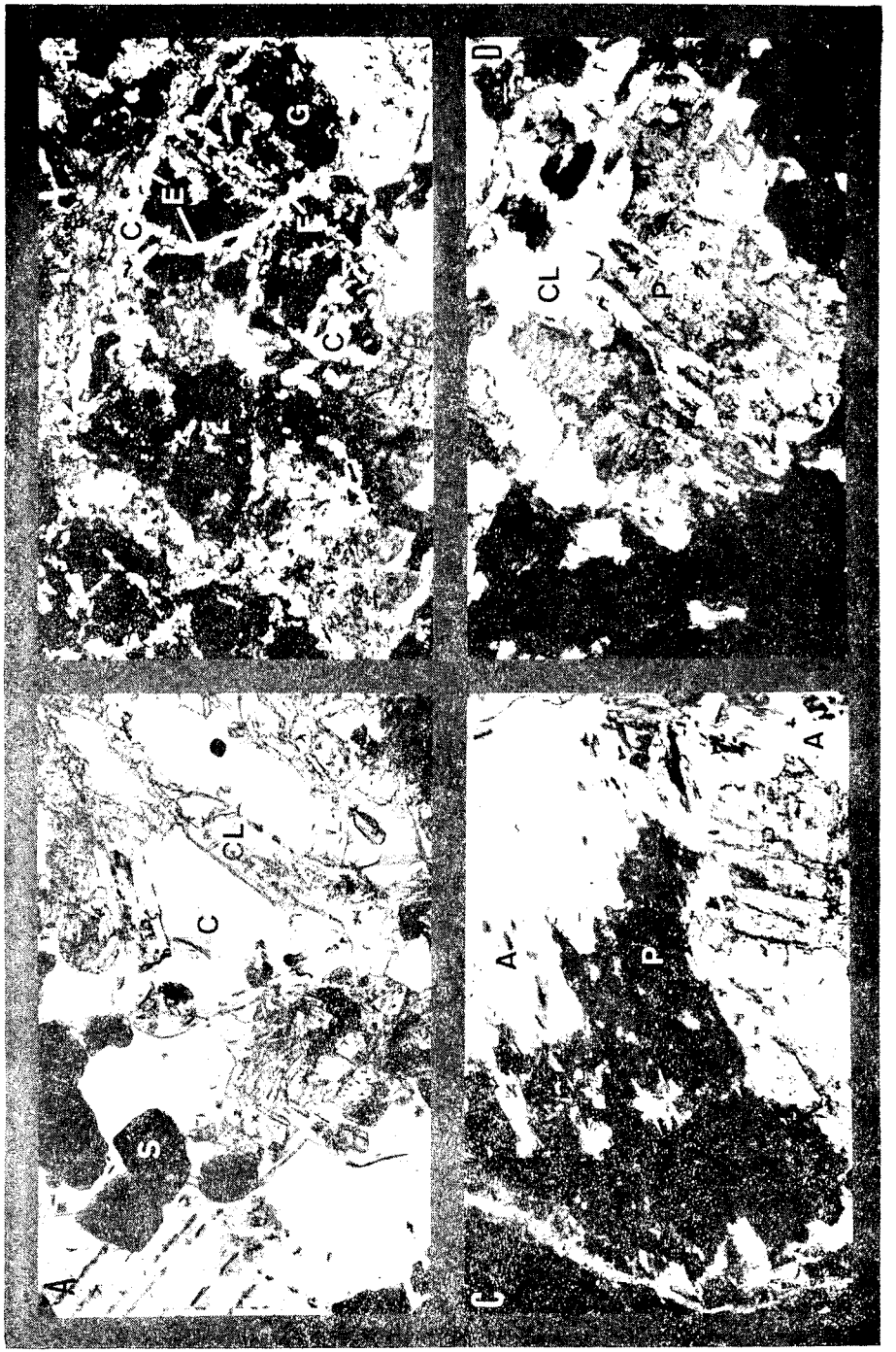

interpret the available evidence to indicate that the various mineral assemblages defining the skarn zones were broadly contemporaneous, although we recognize that this interpretation could be a simplification.

The skarn-marble contact is seldom exposed at Elkhorn. Where exposed it consists of an abrupt (< 1 cm) transition from massive or radiating pyroxene laths to a narrow transition zone of *Cc* + *Dol* + *Fo* + *Sp* marble into the normal *Dol* + *Cc* + *Pe*(Br) + *Fo* ± *Sp* marble (pl. 3-C).

Nodule skarns.—The Nodule skarns are occurrences of pod-like masses of mineralogically zoned skarn of up to 50 cm in diameter. The largest have calcite-bearing cores. The Nodule skarns are concentrically zoned in two distinct sequences (table 2 and pl. 3-D) outward from their centers. The common sequence is: *Cc* + *Sp* + *Clt* → *Sp* + *Clt* → *Clt* ± minor *Chl* → *Gn* → *Gn* + *Px* ± *Vs* ± *Clt*. The outer zone is actually the Massive skarn which encloses the Nodule skarns. The clintonite is texturally primary in these zones, consisting of lath-like grains of variable length, in apparent equilibrium contact with *Sp*, *Gn*, or *Px* (pls. 4-A and 2-A).

Stage II

Stage II is marked by limited replacement of garnet and pyroxene throughout the skarns by hydrous silicates, calcite, and, rarely, quartz (table 1). Small amounts of magnetite and sulfides sometimes accompany this replacement. Several specific replacement assemblages have been observed (table 1), most commonly resulting from replacement of garnet and pyroxene along fractures or at grain margins by epidote and calcite (pl. 4-B) and amphibole (pl. 4-C) respectively. Replacement of aluminous pyroxene by clintonite or biotite occurs along fractures or veinlets within grains or at grain margins (pl. 4-D), although the degree of replacement in any area usually is minor. These occurrences of epidote and clintonite are clearly secondary with respect to *Gn* + *Px* and contrast sharply with their occurrences described earlier as part of stage I.

MINERAL COMPOSITIONS

Representative microprobe mineral analyses of pyroxene, garnet, epidote, and clintonite from stage I skarns and two igneous biotites are presented in tables 3, 4, and 5. Microprobe and data reduction procedures are discussed in appendix 1 and in Bowman (ms). Significant (greater than 5 mole percent change in abundance of one or more components) core-to-

← A. Photomicrograph of the calcite-bearing core of a Nodule skarn with calcite (C), spinel (S), and clintonite (CL). The clintonite laths are in apparent equilibrium contact with spinel and calcite. The Nodule skarn zones progressively from this assemblage through the sequence *Sp* + *Clt* → *Clt* ± minor *Chl* → *Gn* → *Gn* + *Px* ± *Vs*. Crossed nicols. × 16.

B. Photomicrograph of stage II epidote (E) and calcite (C) which have replaced stage I garnet (G) along fractures and grain rims. Crossed nicols. × 6.3.

C. Photomicrograph of stage II amphibole (A) which has partially replaced stage I pyroxene (P). Crossed nicols. × 16.

D. Photomicrograph showing the partial replacement of a single grain of aluminous pyroxene (P) from stage I by stage II clintonite (CL) along fractures, cleavage, and grain rims. Crossed nicols. × 6.3.

TABLE 3
Representative electron-microprobe analyses of skarn pyroxenes

	C13-12[a]	E3-91[a]	C10-38[b]	E11-4[a]	E2-10[c]	E3-78[b]	C11-18[d]	C10-36[d]	E9-46[c]	E9-23[b]	E1-35a[c]	C11-17[b]
SiO_2	51.31	54.09	53.62	50.36	46.91	54.86	41.11	47.77	48.97	52.40	47.96	41.88
TiO_2	0.19	0.01	0.35	0.44	1.09	<0.01	0.64	0.36	1.35	0.04	2.09	0.38
Al_2O_3	0.38	0.87	0.58	1.24	8.68	0.12	15.78	9.62	7.82	0.12	2.90	21.22
[1]Fe_2O_3	-	-	0.09	1.65	4.66	-	7.86	-	1.35	-	0.80	0.75
FeO	17.12	4.68	6.43	10.54	-	1.32	1.61	5.72	2.07	3.60	4.53	-
MnO	< 0.01	< 0.04	n.a.	0.03	n.a.	<0.01	0.01	0.04	n.a.	0.10	0.04	0.03
MgO	7.81	14.76	14.56	10.78	14.01	17.84	9.22	11.29	14.79	16.30	15.10	11.12
CaO	24.32	26.03	25.33	23.94	25.95	26.12	24.44	24.77	24.72	26.41	25.55	26.22
Na_2O	0.12	0.04	0.14	0.36	0.02	0.01	<0.01	0.05	0.06	0.05	0.01	0.01
Total	101.25	100.49	101.09	99.35	101.32	100.26	100.66	99.62	101.13	99.02	98.98	101.61
Si	1.97	1.98	1.98	1.94	1.72	1.98	1.53	1.78	1.78	1.98	1.87	1.53
Al^{IV}	0.02	0.02	0.02	0.06	0.28	<0.01	0.47	0.22	0.22	0.01	0.13	0.47
Al^{VI}	-	0.02	<0.01	-	0.10	-	0.22	0.20	0.11	-	-	0.42
Ti	0.01	<0.01	0.01	0.01	0.03	<0.01	0.02	0.01	0.04	0.01	0.06	0.01
$^1Fe^{+3}$	-	-	<0.01	0.04	0.13	-	0.21	-	0.04	-	0.01	0.02
Fe^{+2}	0.54	0.15	0.21	0.35	-	0.04	0.06	0.18	0.06	0.10	0.15	-
Mn	<0.01	<0.01	n.a.	<0.01	n.a.	<0.01	<0.01	<0.01	n.a.	<0.01	0.01	<0.01
Mg	0.44	0.81	0.80	0.62	0.77	0.96	0.51	0.62	0.80	0.90	0.86	0.59
Ca	0.99	1.02	0.99	0.99	1.02	1.01	0.97	0.99	0.96	1.02	1.00	1.00
Na	<0.01	<0.01	<0.01	<0.01	<0.01	<0.01	<0.01	<0.01	<0.01	<0.01	<0.01	<0.01
$CaMgSi_2O_6$	44.4	82.5	77.4	60.7	74.9	96.0	49.9	59.4	76.2	89.4	79.8	56.7
$CaFeSi_2O_6$	53.7	15.1	21.1	35.9	-	4.0	5.9	17.8	6.0	9.6	13.6	-
$CaAl_2SiO_6$	1.2	2.4	-	-	9.6	-	21.6	21.8	10.8	0.6	-	40.4
$CaFe^{+3}AlSiO_6$	-	-	0.5	2.1	12.6	-	20.6	-	3.5	-	1.1	1.9
$CaTiAl_2O_6$	0.7	-	1.0	1.3	2.9	-	2.0	1.0	3.5	0.4	5.5	1.0

[1] Fe_2O_3 calculated by charge balance n.a. not analyzed

Mineral Assemblages: a = Gn + Px + Pg; b = Gn + Px + Ce; c = Gn + Px + Vs + Clt; d = Px + Clt + Sp + Ce; e = Px + Sp + Ce; f = Gn + Px + Clt + Sp + Ce; g = Gn + Px + Sp + Ce; h = Gn + Px + Clt + Ce

	E11-4c[a]	C11-21[c]	C11-7a[d]	C12-39b[f]	C12-37b[f]	C13-15[n]	C12-31n[d]	E1-34b[f]	C3-16a[g]	C2-21[g]	C3-26d[h]	E1-29[f]
SiO_2	54.08	47.31	51.46	43.92	46.15	50.97	49.78	48.52	43.84	45.76	47.58	46.59
TiO_2	0.01	0.58	0.58	0.69	1.01	0.34	0.04	0.37	0.36	0.06	0.09	0.06
Al_2O_3	0.93	11.82	3.40	12.53	11.19	0.66	7.62	9.82	15.85	14.33	9.51	12.48
$^1Fe_2O_3$	0.72	-	0.38	4.86	2.56	-	0.36	1.46	1.80	0.72	4.00	1.42
FeO	2.61	1.03	2.48	1.97	0.98	18.16	1.63	0.66	0.97	0.65	0.66	0.96
MnO	n.a.	n.a.	n.a.	< 0.01	0.04	0.09	0.01	0.04	n.a.	n.a.	n.a.	0.03
MgO	15.76	12.67	15.71	11.34	13.83	6.74	14.05	14.06	11.08	12.06	13.21	12.23
CaO	26.00	26.01	25.88	25.47	24.20	23.79	25.39	25.73	25.76	25.42	25.78	25.68
Na_2O	0.06	0.02	n.a.	n.a.	n.a.	< 0.01	< 0.01	< 0.01	0.02	0.01	< 0.01	< 0.01
Total	100.17	99.44	99.89	100.78	99.96	100.75	98.87	100.66	99.68	99.01	100.83	99.45
Si	1.98	1.73	1.89	1.64	1.68	1.98	1.83	1.76	1.62	1.68	1.74	1.71
Al^{IV}	0.02	0.27	0.11	0.36	0.32	0.02	0.17	0.24	0.38	0.32	0.26	0.29
Al^{VI}	0.02	0.24	0.04	0.20	0.19	0.01	0.16	0.18	0.31	0.30	0.15	0.25
Ti	< 0.01	0.02	0.02	0.02	0.03	0.01	0.01	0.01	0.01	< 0.01	< 0.01	< 0.01
$^1Fe^{+3}$	0.02	-	0.01	0.12	0.07	-	0.01	0.04	0.05	0.02	0.11	0.04
Fe^{+2}	0.08	0.03	0.08	0.05	0.03	0.59	0.05	0.02	0.03	0.02	0.02	0.03
Mn	n.a.	n.a.	n.a.	< 0.01	< 0.01	< 0.01	< 0.01	< 0.01	n.a.	n.a.	n.a.	< 0.01
Mg	0.86	0.69	0.86	0.61	0.75	0.39	0.77	0.76	0.61	0.66	0.72	0.67
Ca	1.02	1.02	1.01	1.00	0.97	0.99	1.00	1.00	1.02	1.00	1.01	1.01
Na	< 0.01	< 0.01	-	-	-	< 0.01	< 0.01	0.01	0.01	< 0.01	< 0.01	< 0.01
$CaMgSi_2O_6$	87.8	70.4	85.1	61.2	70.1	39.0	77.7	75.2	60.2	66.3	72.0	67.9
$CaFeSi_2O_6$	8.2	3.1	7.9	4.9	2.8	59.0	5.1	2.0	3.0	2.0	2.0	3.1
$CaAl_2SiO_6$	2.0	24.5	4.0	20.1	17.8	1.0	16.2	17.8	30.7	29.7	15.0	25.0
$CaFe^{+3}AlSiO_6$	2.0	-	1.0	11.8	6.5	-	1.0	4.0	5.1	2.0	11.0	4.0
$CaTiAl_2O_6$	-	2.0	2.0	2.0	2.8	1.0	-	1.0	1.0	-	-	-

[1] Fe_2O_3 calculated by charge balance

n.a. not analyzed

Mineral Assemblages: a = Gn + Px + Pg; b = Gn + Px + Cc; c = Gn + Px + Vs + Clt; d = Px + Clt - Sp + Cc; e = Px + Sp + Cc; f = Gn + Px + Clt + Sp + Cc; g = Gn + Px + Sp + Cc; h = Gn + Px + Clt + Cc

TABLE 4

Representative electron-microprobe analyses of skarn garnets

	C13-12[a]	C13-15[a]	E3-90[a]	E3-91[a]	E3-78[b]	E9-23[b]	E1-35a[c]	C10-22[b]	C11-17[b]	C10-38[b]	E11-4[a]	C12-39b[f]
SiO_2	34.94	34.83	38.24	38.12	34.64	37.91	33.40	37.81	37.26	38.22	39.87	36.68
TiO_2	0.62	0.66	0.08	0.04	0.06	0.49	2.39	0.51	0.30	0.39	-	0.56
Al_2O_3	7.91	7.42	17.07	16.53	5.67	13.38	4.56	14.46	17.02	14.05	21.99	12.76
Fe_2O_3	18.22	19.04	7.51	8.25	22.39	11.02	21.01	10.56	7.15	10.56	1.59	15.22
FeO	1.94	1.93	0.98	0.57	0.96	0.42	3.37	-	0.16	-	-	0.35
MnO	1.62	0.66	0.41	0.38	0.02	0.24	0.04	n.a.	0.18	0.22	n.a.	0.05
MgO	0.04	0.03	0.09	0.09	0.04	0.32	0.30	0.43	0.06	0.09	0.06	0.43
CaO	33.30	34.05	35.89	35.90	34.60	35.89	33.70	33.76	37.04	36.41	37.08	35.39
Total	98.59	98.62	100.27	99.88	98.38	99.67	98.77	99.53	99.17	99.34	100.59	101.44
*H_2O	2.06	2.11	0.92	0.80	2.01	0.62	2.54	0.38	1.05	-	-	0.81
Si	2.73	2.72	2.88	2.90	2.73	2.92	2.66	2.95	2.87	2.96	3.00	2.89
Al^{IV}	-	-	-	-	-	-	-	-	-	-	-	-
Al^{VI}	0.74	0.68	1.52	1.48	0.53	1.22	0.43	1.33	1.53	1.33	1.91	1.18
Ti	0.04	0.04	0.01	0.01	-	0.03	0.14	0.03	0.02	0.02	0.01	0.03
Fe^{+3}	1.18	1.24	0.48	0.52	1.47	0.71	1.29	0.62	0.42	0.62	0.09	0.76
Fe^{+2}	0.14	0.14	0.07	0.04	0.07	0.03	0.23	-	0.01	-	-	0.02
Mn	0.05	0.04	0.03	0.03	0.01	0.02	0.01	n.a.	0.01	0.02	n.a.	0.01
Mg	0.01	0.01	0.01	0.01	0.01	0.04	0.04	0.05	0.01	0.01	0.01	0.05
Ca	2.84	2.85	2.90	2.92	2.92	2.96	2.87	2.99	3.01	3.03	2.99	2.96
*H	1.10	1.13	0.47	0.41	1.09	0.32	1.37	0.20	0.54	-	-	0.44
$Ca_3R^{+2}TiSi_3O_{12}$	1.7	1.8	-	-	-	1.5	6.3	1.5	0.8	1.1	-	1.4
$Ca_3Al_2Si_3O_{12}$	33.7	30.8	72.9	67.7	23.9	59.2	18.9	65.4	73.2	65.5	95.5	56.8
$Ca_3Fe_2Si_3O_{12}$	53.3	56.1	21.4	27.1	67.0	34.2	57.7	30.4	20.9	31.4	4.0	36.2
$Ca_3Mn_2Si_3O_{12}$	2.2	1.9	1.2	1.2	-	0.7	-	-	0.6	0.7	-	-
$Mg_3Al_2Si_3O_{12}$	-	-	0.6	0.6	-	1.8	5.7	1.0	-	-	0.5	1.9
$R_3^{+2}R_2^{+3}H_{12}O_{12}$	9.1	9.4	3.9	3.4	9.1	2.6	11.4	1.7	4.5	1.3	-	3.7

*H_2O calculated by filling IV site = 3.00 atoms n.a. not analyzed

Mineral Assemblages: a = Gn + Px + Pg; b = Gn + Px + Ce; c = Gn + Px + Vs + Clt; d = Px + Clt + Sp + Ce; e = Px + Sp + Ce; f = Gn + Px + Clt + Sp + Ce; g = Gn + Px + Sp + Ce; h = Gn + Px + Clt + Ce

	C12-37b[f]	E1-34b[f]	C3-16a[g]	C2-21[g]	C3-26d[h]	E2-2[b]	E1-35d[c]	E1-29[f]	E2-50[b]	E2-56a[a]	E9-37b[a]	X1-6[c]
SiO_2	37.48	38.66	38.31	38.09	37.29	39.04	33.21	38.51	36.26	38.58	37.14	39.01
TiO_2	1.10	0.70	0.07	0.70	1.03	n.a.	2.41	0.53	0.49	0.71	0.62	0.38
Al_2O_3	12.81	16.35	16.70	18.10	14.67	19.50	4.57	17.91	3.62	17.07	11.40	18.41
Fe_2O_3	12.43	7.49	7.97	4.52	8.92	3.38	23.60	5.61	25.73	6.50	15.06	4.36
FeO	0.31	-	-	-	0.46	-	0.84	-	0.42	1.85	0.30	0.12
MnO	0.09	0.05	n.a.	n.a.	n.a.	1.24	0.02	n.a.	0.04	0.65	0.40	0.37
MgO	0.52	0.53	0.26	0.61	0.43	n.a.	0.40	0.44	0.18	0.12	0.03	0.46
CaO	35.52	36.70	36.73	36.53	35.88	36.94	33.99	37.05	33.44	35.03	35.65	36.21
Total	100.26	100.48	100.04	98.55	98.68	100.10	99.04	100.05	100.18	100.51	100.60	99.32
*H_2O	0.23	0.39	0.47	0.71	0.85	0.49	1.22	0.63	-	0.10	0.50	-
Si	2.96	2.95	2.94	2.91	2.89	2.94	2.83	2.92	3.00	2.99	2.93	3.00
Al^{IV}	-	-	-	-	-	-	-	-	-	-	-	-
Al^{VI}	1.19	1.47	1.51	1.63	1.34	1.73	0.35	1.60	0.36	1.51	1.06	1.67
Ti	0.06	0.04	0.01	0.04	0.06	n.a.	0.06	0.03	0.03	0.04	0.04	0.02
Fe^{+3}	0.68	0.43	0.46	0.26	0.52	0.21	1.52	0.32	1.60	0.38	0.90	0.26
Fe^{+2}	0.02	-	-	-	0.03	-	0.06	-	0.03	0.12	0.02	0.01
Mn	0.01	0.01	n.a.	n.a.	n.a.	0.08	0.01	n.a.	0.01	0.04	0.03	0.03
Mg	0.06	0.06	0.03	0.07	0.05	n.a.	0.02	0.05	0.02	0.02	0.01	0.04
Ca	2.98	3.00	3.02	2.99	2.98	2.98	2.98	3.01	2.97	2.91	3.02	2.98
*H	0.16	0.20	0.24	0.36	0.44	0.25	0.66	0.32	-	0.05	0.26	-
$Ca_3R^{+2}TiSi_3O_{12}$	3.0	2.0	-	1.9	2.9	-	2.9	1.5	1.6	1.9	1.8	1.1
$Ca_3Al_2Si_3O_{12}$	58.7	72.2	74.0	79.1	64.3	84.7	16.7	77.8	17.8	75.1	51.9	83.1
$Ca_3Fe_2Si_3O_{12}$	36.0	23.1	22.5	15.5	28.1	9.3	73.8	17.0	79.4	19.5	42.8	13.1
$Ca_3Mn_2Si_3O_{12}$	-	-	-	-	-	3.9	-	-	-	2.4	1.3	1.5
$Mg_3Al_2Si_3O_{12}$	1.0	1.0	1.5	0.5	1.0	-	1.1	1.0	1.2	0.7	-	1.0
$R_3^{+2}R_2^{+3}H_{12}O_{12}$	1.3	1.7	2.0	3.0	3.7	2.1	5.5	2.7	-	0.4	2.2	0.2

* H_2O calculated by filling IV site = 3.00 atoms. n.a. not analyzed

Mineral Assemblages: a = Gn + Px + Pg; b = Gn + Px + Ce; c = Gn + Px + Vs + Clt; d = Px + Clt + Sp + Ce; e = Px + Sp + Ce; f = Gn + Px + Clt + Sp + Ce; g = Gn + Px + Sp + Ce; h = Gn + Px + Clt + Ce

TABLE 5

Representative electron-microprobe analyses of skarn epidotes and clintonites and igneous biotites

	Epidote					Clintonite			Biotite	
	Stage I			Stage II						
	C8-11	C9-38	E2-56a	E11-4c	C2-30	C12-37b	C12-39b	E1-29	X1-9	C3-22
SiO_2	37.79	37.91	38.06	39.40	38.29	17.63	16.91	17.65	39.70	38.56
TiO_2	0.15	0.48	0.08	0.04	0.72	0.19	< 0.01	0.05	0.04	0.06
Al_2O_3	24.02	22.98	27.06	30.85	24.00	42.13	43.62	40.61	14.17	16.14
$^1Fe_2O_3$	11.93	13.30	8.99	4.03	12.01	2.86	3.20	3.35	-	-
FeO	-	-	-	-	-	-	-	0.42	22.01	18.59
MnO	na	na	0.09	0.06	0.12	na	na	na	0.15	0.31
MgO	na	0.09	0.01	na	0.11	21.13	20.02	19.84	11.38	13.20
CaO	23.99	23.73	23.98	24.71	23.98	12.71	12.64	12.25	< 0.01	< 0.01
Na_2O	na	na	na	na	na	na	na	na	< 0.01	< 0.01
K_2O	na	na	na	na	na	na	na	na	7.11	7.82
F	0.20	na	0.01	0.04	0.05	0.44	0.70	0.27	0.20	0.14
Cl	< 0.01	na	< 0.01	< 0.01	< 0.01	0.17	0.01	0.14	0.85	< 0.01
$^2H_2O^+$	1.81	1.88	1.92	1.94	1.90	4.02	3.93	4.03	3.62	3.97
Total	99.89	100.37	100.18	101.07	101.18	101.28	101.03	98.61	99.23	98.79
Si	2.98	3.00	2.97	2.99	3.00	4.90	4.72	5.04	3.02	2.90
Al^{IV}	0.02	-	0.03	0.01	-	11.10	11.28	10.96	0.98	1.10
Al^{VI}	2.24	2.15	2.45	2.75	2.22	2.69	3.06	2.72	0.25	0.33
Ti	0.01	0.03	< 0.01	< 0.01	0.04	0.04	< 0.01	0.01	< 0.01	< 0.01
$^1Fe^{+3}$	0.71	0.80	0.52	0.23	0.70	0.54	0.61	0.72	-	-
Fe^{+2}	-	-	-	-	-	-	-	0.10	1.40	1.17
Mn	na	na	0.01	< 0.01	0.01	na	na	na	0.01	0.02
Mg	na	0.01	< 0.01	na	0.01	8.75	8.32	8.45	1.29	1.48
Ca	2.02	2.02	2.02	2.01	2.02	3.78	3.78	3.75	< 0.01	< 0.01
Na	na	na	na	na	na	na	na	na	< 0.01	< 0.01
K	na	na	na	na	na	na	na	na	0.69	0.75
F	0.05	na	< 0.01	0.01	0.01	0.39	0.63	0.25	0.05	0.03
Cl	< 0.01	na	< 0.01	< 0.01	< 0.01	0.08	< 0.01	0.07	0.11	< 0.01
^2OH	0.95	1.00	1.00	0.99	0.99	7.53	7.37	7.68	1.84	1.97

$^1Fe_2O_3$ calculated by charge balance ^2H_2O calculated from mineral stoichiometry na not analyzed

rim compositional zoning exists in a few of the garnets and pyroxenes analyzed. In these cases, the analyses reported in tables 3 and 4 are analyses of rims of physically touching minerals, where compositional heterogeneities are usually less than 5 mole percent in any major component molecule.

Pyroxene

Skarn pyroxenes are characterized by wide variation in the relative proportions of the components diopside (Di: $CaMgSi_2O_6$), hedenbergite (Hd: $CaFeSi_2O_6$), Al–tschermaks (AlTs: $CaAl_2SiO_6$), Fe–tschermaks (FeTs: $CaFe^{+3}AlSiO_6$), and Ti–tschermaks (TiTs: $CaTiAl_2O_6$) typically in this order of abundance (table 3). The pyroxenes contain minor TiO_2 (< 1.5 wt percent for all but two samples) and only traces of Mn and Na. All analyzed pyroxenes contain close to one Ca atom per six oxygen atoms.

Figure 3 is a plot of all pyroxene analyses in terms of the four dominant molecules. TiTs molecule was almost always less than 2 percent and has been neglected in these plots except where plotted as part of total tschermaks component. Skarn pyroxenes are quite variable in composition but usually belong to either a Di–Hd series ($<$ 10 percent Ts; 0-60 percent Hd; $>$ 40 percent Hd rare) or a Di–Ts series ($\leqslant$ 42 percent AlTs; $\leqslant$ 22 percent FeTs). There are no striking compositional distinctions between pyroxenes from the Massive and Contact skarn types, although

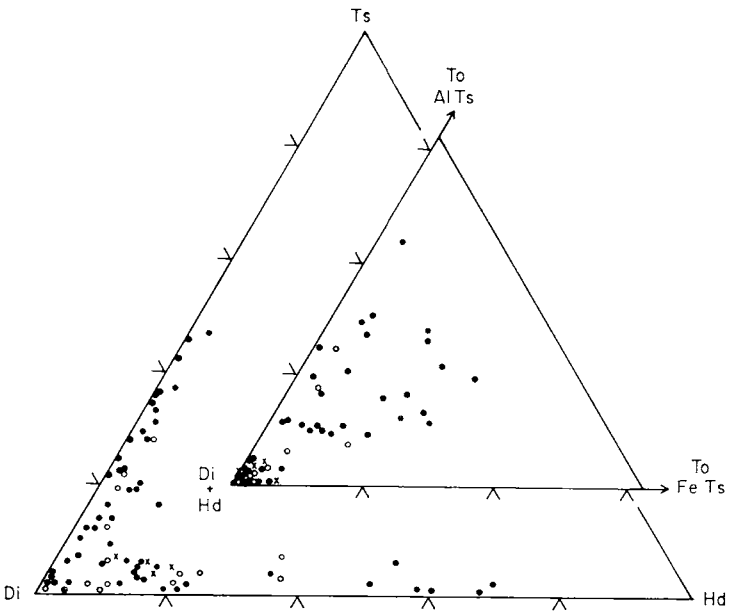

Fig. 3. Pyroxene compositions from the Massive (●), Contact (○), and Nodule (x) skarns expressed in terms of molar proportions of diopside (Di) — $CaMgSi_2O_6$, hedenbergite (Hd) — $CaFeSi_2O_6$, Al–tschermaks (AlTs) — $CaAl_2SiO_6$, and Fe–tschermaks (FeTs) — $CaFe_2SiO_6$ molecules, calculated from electron-microprobe analyses. Mineral analyses are given in Bowman (ms).

pyroxenes from the Nodule skarns have significantly lower maximum Ts contents and less variable Fe(Fe + Mg) ratios than those from the other two skarn types. The low Ts pyroxenes from the uncommon Massive skarns which contain quartz are the most iron-rich. Pyroxenes from areas I through III (figs. 1 and 2) show no systematic change in total iron (reflected either as increasing Hd or FeTs component) or tschermaks component toward the intrusive contact.

Figure 4 is an ACF diagram on which are plotted the Di–Ts series pyroxenes and some clintonite analyses. Although there is wide variation in the tschermaks composition of all pyroxenes analyzed, pyroxenes (samples C12-37b, C12-39b, table 3) associated with *Gn* + *Sp* + *Clt* ± *Cc* assemblages (open circles) have a much more restricted range of tschermaks contents (16-21 mole percent). The clintonites in these samples also have a restricted range of compositions (see below). Neither pyroxene nor clintonite has a truly constant composition, indicating that their compositions were not strictly buffered by the mineral assemblage. Pyroxenes from *Gn* + *Px* + *Pg* assemblages have compositions (open triangles) restricted to much lower total tschermaks contents (3-10 mole percent) and

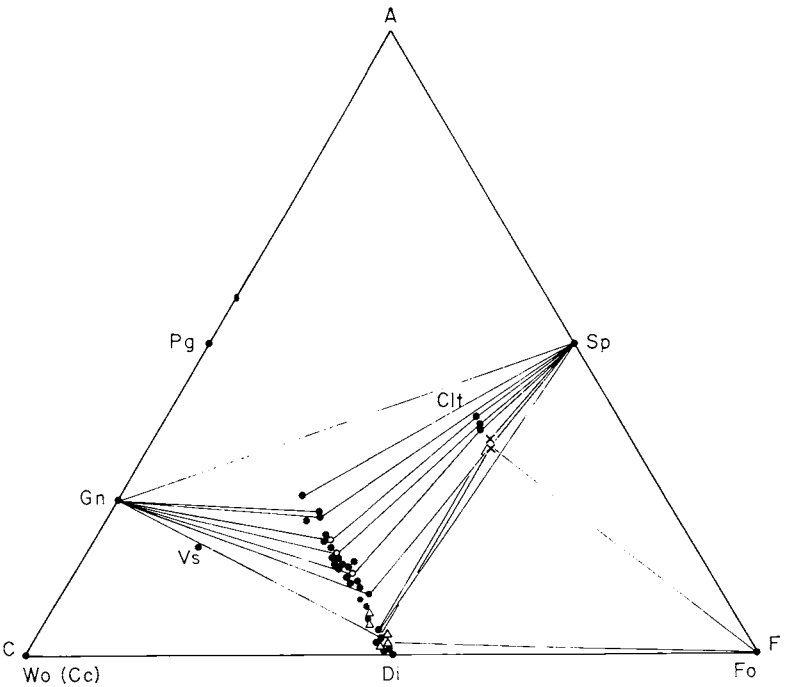

Fig. 4. ACF diagram illustrating the variation in pyroxene composition as a function of skarn mineralogy. Tie-lines illustrate maximum variation in pyroxene composition for *Px* + *Gn*, *Px* + *Gn* + *Sp*, *Px* + *Sp* and *Px* + *Gn* + *Sp* + *Clt* assemblages (open circles denote pyroxenes from this assemblage). Open triangles represent pyroxene compositions from *Gn* + *Px* + *Pg* assemblages. Clintonite compositions from *Px* + *Clt* + *Sp* + *Fo* assemblages are plotted as Xs.

to a much smaller compositional range as well. The restricted ranges of pyroxene and clintonite compositions in these lower variance assemblages are consistent with a reasonable approach to equilibrium for these skarn assemblages.

Garnet

Representative garnet microprobe analyses (table 4) indicate that important garnet components are grossular, andradite, and hydrogarnet in that order, with other components less than 2 percent (fig. 5). Hydrogarnet contents are less than 10 mole percent in all but seven out of 68 garnet analyses. Compositions of massive skarn garnets range from Gr(96) to Gr(18), but most compositions are between Gr(90) and Gr(65). Almost all the garnets with andradite contents greater than 50 mole percent are from either low-aluminum pyroxene- and plagioclase-bearing assemblages or the Nodule skarns. Nodule skarn garnets are restricted to a relatively narrow composition range of Gr(28) to Gr(18). All available analyses of Contact skarn garnets indicate grossular contents of 55 mole percent or greater.

Compositions of coexisting garnet–pyroxene pairs have been plotted in figure 6, a graph of X_{Ad} versus X_{Hd}. At constant P-T, the partitioning of Fe between the two phases (X_{Ad}/X_{Hd}) will be a function of both $f(O_2)$ and bulk composition (Brown, ms), as indicated by the arrows superimposed on figure 6. Several distinct groupings of the data are apparent.

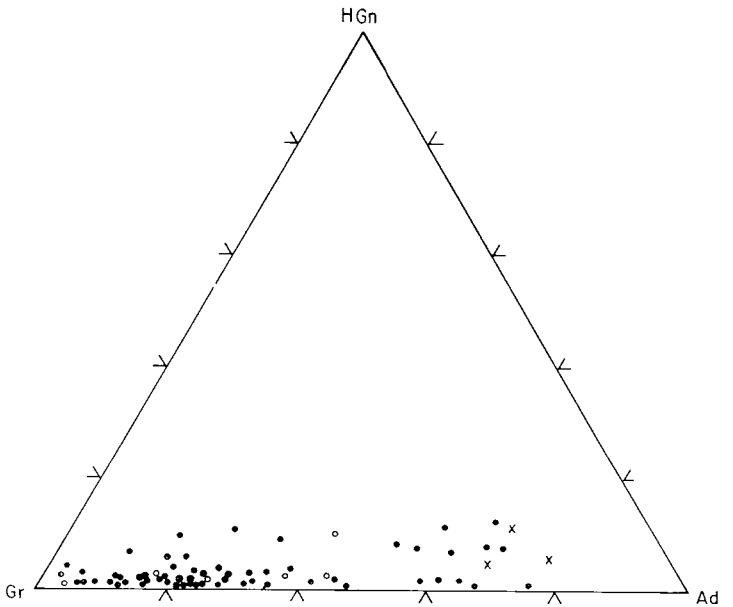

Fig. 5. Elkhorn garnet compositions expressed in terms of molar proportions of grossular (Gr) — $Ca_3Al_2Si_3O_{12}$, andradite (Ad) — $Ca_3Fe_2Si_3O_{12}$, and hydrogarnet (HGn) — $R_3R_2H_{12}O_{12}$ molecules, calculated from electron-microprobe analyses. Mineral analyses are given in Bowman (ms). Symbols as in figure 3.

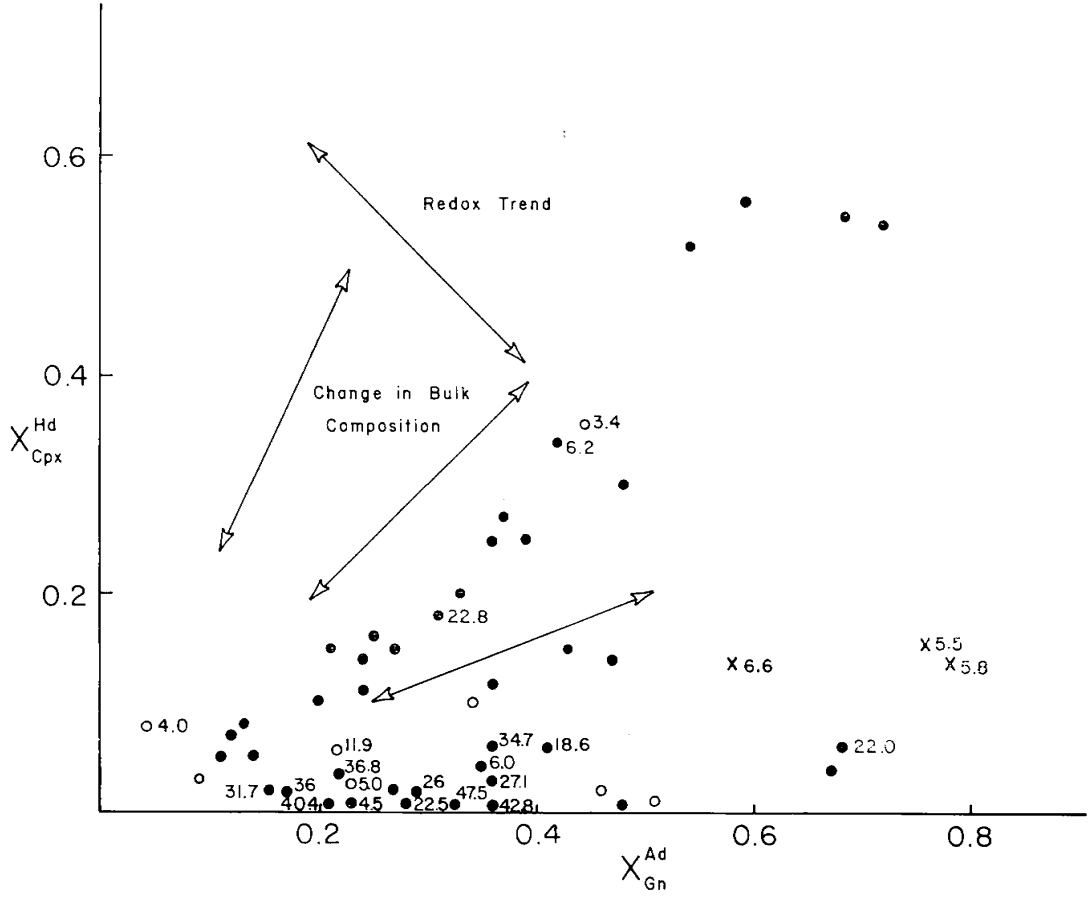

Fig. 6. Plot of mole fraction hedenbergite in pyroxene versus mole fraction andradite in garnet for garnet–pyroxene pairs from the Elkhorn skarns. Symbols as in figure 3. Mole percent total tschermaks component in pyroxenes (if greater than 3 mole percent) is indicated immediately to the right or left of sample location. Theoretical trends due solely to variable $f(O_2)$ or to variable total iron content are also marked by the arrows for reference.

Garnets and nearly binary Di–Hd pyroxenes (dominantly from Massive skarn) define a linear spectrum of bulk compositions with a relatively constant $(X_{Ad}/X_{Hd}) = 1.25$, implying relatively constant $f(O_2)$ values. Garnet–pyroxene pairs from the Nodule skarns define a distinct $(X_{Ad}/X_{Hd}) = 3.8$ to 4.0 suggesting higher $f(O_2)$ values. In contrast, pairs from some Massive and all Contact skarns define a distinct linear array with variable (X_{Ad}/X_{Hd}) from 1.25 to 3.8, suggesting variable $f(O_2)$ values. These distinct groupings contrast with the more coherent iron partitioning observed for garnet–pyroxene pairs in several W- and Cu-bearing skarns (Brown, ms; Newberry, ms; Cook, ms). Pyroxenes in these types of skarns are essentially diopside–hedenbergite solid solutions. In contrast, many of the low-Fe^{+2} pyroxenes at Elkhorn which define variable (X_{Ad}/X_{Hd}) values contain significant (> 5 mole percent) total tschermaks content (fig. 6), and it is possible that tschermaks component disrupts the iron partitioning between garnet and pyroxene. Because both tschermaks component and iron partitioning between garnet and pyroxene are functions of $a(SiO_2)$ in common skarn assemblages at Elkhorn (Bowman, ms; Brown, ms), the observed variations in iron partitioning may not necessarily indicate variable $f(O_2)$.

Clintonite

Compositions of stage I clintonites are variable (table 5) but are correlated with skarn mineralogy (fig. 4). For example, silicon contents in clintonites associated with *Px* + *Sp* (table 4, sample E1-29) and *Px* + *Fo* assemblages range from 5.08 to 5.35 atoms per 40 oxygens, while silicon contents of clintonites associated with *Gn* + *Px* + *Sp* ± *Cc* (samples C12-37b and C12-39b) range from 4.72 to 4.95 atoms per 40 oxygens. Compositions of clintonites associated with *Px* + *Sp* and *Px* + *Fo* lie close to the MgSi-rich end of the clintonite solid solution series synthesized by Olesch (1975) and are close in composition (with respect to Si:Al ratio) to clintonites from contact metamorphosed aluminous marbles at the northern margin of the Boulder Batholith (Rice, 1979). The more aluminous clintonites are associated with the more aluminous bulk composition represented by the *Gn* + *Px* + *Sp* + *Clt* ± *Cc* assemblage. The restriction of the chemical compositions of both clintonite and pyroxene (fig. 4) in the presence of *Gn* + *Sp* + *Cc* suggests that these four and five-phase associations may be equilibrium assemblages.

Epidote and Biotite

Microprobe analyses of representative epidote and igneous biotite samples are shown in table 5. Compositions of primary epidotes from the *Px* + *Ep* + *Sc* assemblages range from 8 to 27 mole percent pistacite component. Epidotes that replace garnet during stage II have a similar range in composition (10-26 mole percent pistacite). During the replacement of garnet, iron is preferentially incorporated into epidote relative to garnet with X_{Ad} values up to 0.25. Epidotes that replace garnets with $X_{Ad} > 0.35$ are depleted relatively in iron (for example, sample C13-12).

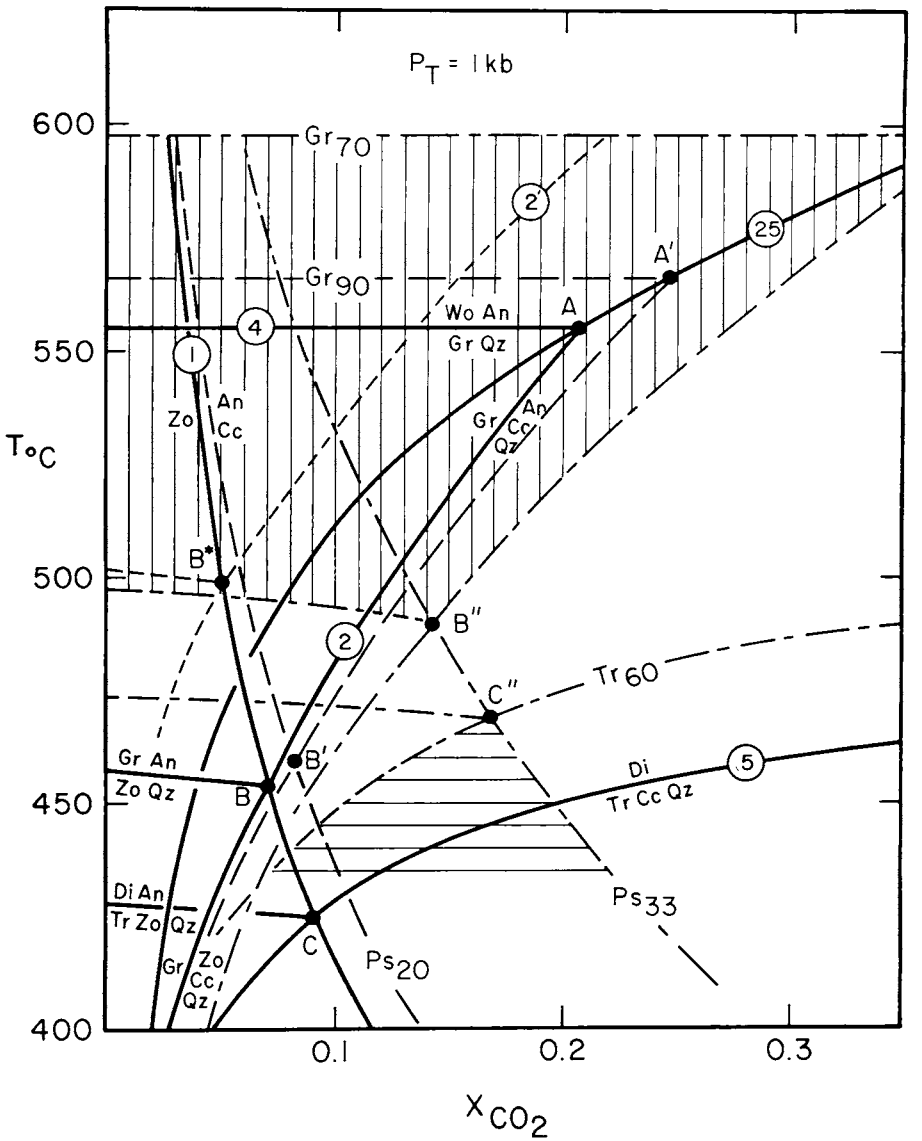

Fig. 7. Isobaric T-X(CO_2) diagram with selected equilibria from the model system CaO–Al_2O_3–SiO_2–H_2O–CO_2 (solid lines) relevant to the first two stages of skarn formation at Elkhorn. The vertical-striped pattern illustrates limits of temperature for stage I of skarn development, based on *Gn* + *Pg* and *Gn* + *Qz* assemblages. The horizontal-striped pattern illustrates upper temperature and X(CO_2) limits for stage II of skarn development, based on the assemblage *Ep* + *Amp* + *Cc* + *Qz*. Abbreviations are: zoisite (*Zo*), anorthite (*An*), pistacite (*Ps*). The effects of progressive solid solution in garnet, epidote, and plagioclase on the positions of these equilibria are also illustrated for $X_{Gr}^{Gn} = 0.9$, $X_{An}^{Pg} = 0.8$, and $X_{Ps}^{Ep} = 0.2$ (long-dashed lines) and $X_{Gr}^{Gn} = 0.7$, $X_{An}^{Pg} = 0.8$, and $X_{Ps}^{Ep} = 0.33$ (long-dashed/short-dashed lines). The shift in equilibrium 5 (long-dashed/short-dashed line) was calculated using the compositions $X_{Oli-Tr}^{Amp} = 0.60$ and $X_{Di}^{Px} = 0.60$. Methods of calculation of these shifts are discussed in the appendix. The effect of $a(SiO_2) < 1.0$ on garnet stability in H_2O–CO_2 fluids is illustrated by the shift of reaction 2 (short dashed line) upon reduction of log $a(SiO_2)$ to −1.0. Sources for equilibria are reaction 1, Johannes and Orville (1972); reaction 2, Gordon and Greenwood (1971); reaction 4, Newton (1966) and Boettcher (1970); reaction 5, Kerrick (1974) and Slaughter, Kerrick, and Wall (1975); reaction 25, Greenwood (1967b); and other reactions, Kerrick (1974).

Analyses of two biotites from the Black Butte stock have also been included in table 5. These biotite compositions have been used to estimate maximum $f(O_2)$ values in potassium feldspar-absent quartz diorites of the Black Butte stock.

PHYSICAL-CHEMICAL CONDITIONS OF EARLY SKARN FORMATION

Reasonably close definition of P-T conditions of skarn formation is a necessary first step to define limits to fluid compositional parameters and to construct realistic geochemical models of skarn processes. The ultimate objective to defining P-T conditions is the determination of the speciation and composition of the skarn fluids, when the necessary activity-composition relationships at elevated P-T become sufficiently well known. Some of the intensive variables for the first two stages of skarn formation can be limited by application of appropriate phase equilibria in the model systems $CaO–MgO–Al_2O_3–SiO_2–H_2O–CO_2$ and Ca–Fe–Si–C–O–H to observed skarn mineral assemblages. We do not imply by these applications that these equilibria represent the actual reactions that form the skarn or that convert one zone to another. These applications assume local equilibrium within skarn zones and at zone boundaries. The effects of solid solutions on phase equilibrium surfaces are calculated with activity data where available, or by assuming ideal ionic solution models, as detailed in appendix 1 and Bowman (ms). Only partial experimental and thermochemical data are available for either vesuvianite or clintonite. The calculations of phase equilibria relevant to mineral assemblages containing clintonite and vesuvianite are therefore approximate.

Only wide limits can be placed on temperature and fluid compositions for stages III and IV. Therefore we will be concerned here with the physical-chemical conditions for formation of stages I and II.

Pressure

Bowman and Essene (1982) inferred $P_f = P_T = 1.0 \pm 0.3$ kb for thermal metamorphism in the Black Butte Stock aureole based on the presence of *And* + *Kfs* and *Gr* + *Qz* in metamorphosed pelites and calc-pelites, respectively. This estimate of load pressure is consistent with estimates of overburden in the area (Klepper, Weeks, and Ruppel, 1957). Skarn formation was subsequent to contact metamorphism but, as will be shown, occurred at temperatures less than 75°C or so below the thermal peak (600°C) of contact metamorphism (Bowman and Essene, 1982). During the time period between contact metamorphism and the early stages of metasomatism, changes in P_T were unlikely, and $P_f = P_T = 1$ kb is assumed for formation of stages I and II.

Temperature

Minimum temperature for stage I skarns is defined by the presence of *Pg* + *Gn* assemblages which occur up to 12 m from the intrusive contact. A minimum temperature of 450°C (invariant point B) at 1 kb P_f is indicated in the Fe-free system (fig. 7) from the intersection of:

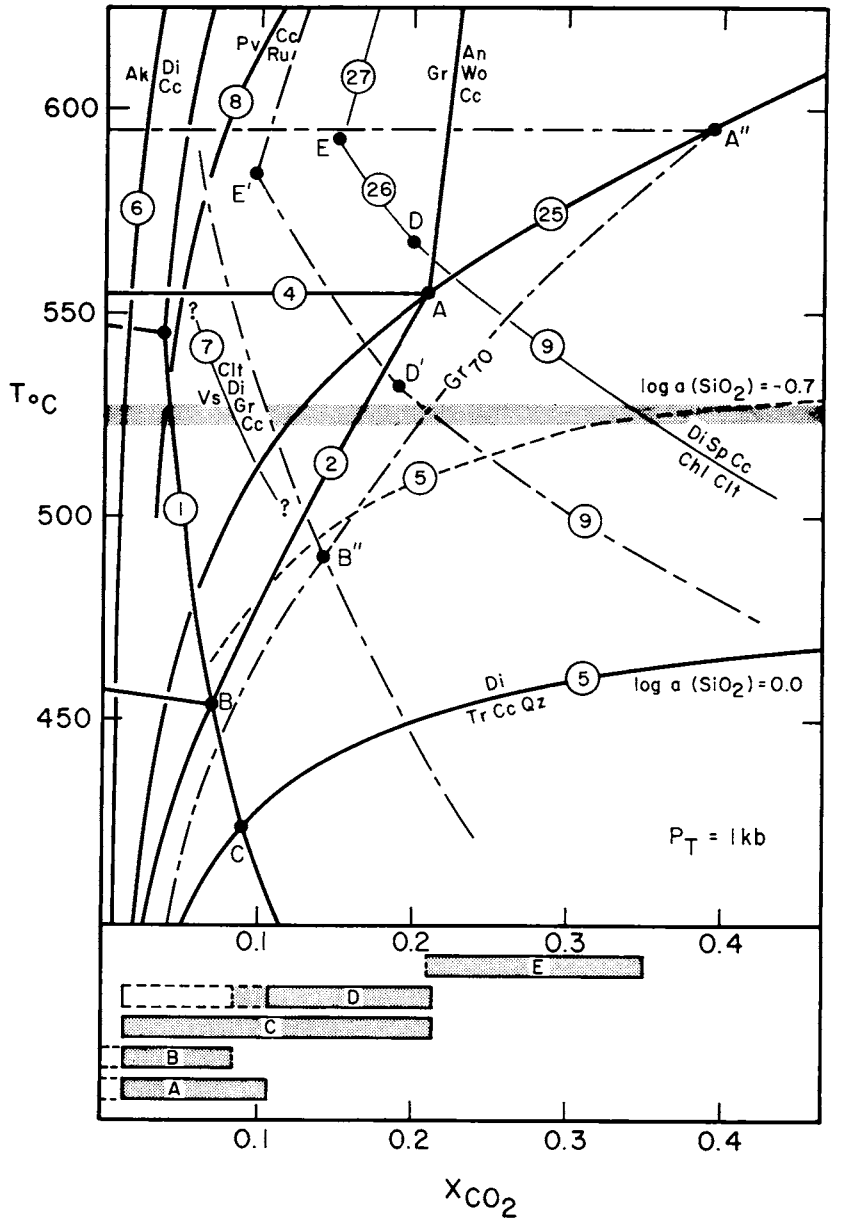

Fig. 8. Isobaric T-X(CO_2) diagram with relevant equilibria from the system CaO–MgO–Al_2O_3–SiO_2–H_2O–CO_2 which define X(CO_2) limits in the Elkhorn skarns. Abbreviations are akermanite (*Ak*), rutile (*Ru*). Sources for the equilibria are as in figure 7 and reaction 6, Zharikov, Shmulovich, and Bulator (1977); reaction 7, estimated from topological analysis using the experimental data of Hochella and others (1982) for the stability of Mg–vesuvianite plus quartz and entropy estimates from Valley and others (ms); reaction 8, Shedlock and Essene (1979); reaction 5, Kerrick (1974); reaction 9, Rice (1979) and Bowman and Essene (1979); and reactions 26 and 27, Bowman and Essene (1979). Not all equilibria associated with each invariant point (for example, points D and E) have been plotted for clarity. The effects of progressive solid solution in garnet, epidote, and plagioclase on the calc-silicate equilibria are from figure 7. Shifts in reactions (9), (26), and (27) were calculated with a(Di) = 0.55, a(Sp) = 0.75, a(Clt) =

$$2\ \text{Zo} + \text{CO}_2 = 3\ \text{An} + \text{H}_2\text{O} \quad (1)$$

$$\text{An} + 2\ \text{Cc} + \text{Qz} = \text{Gr} + 2\ \text{CO}_2 \quad (2)$$

This invariant point, corrected for typical skarn garnet ($Gr_{70\text{-}85}$), epidote ($Ps_{26\text{-}20}$), and plagioclase ($An_{75\text{-}85}$) compositions, raises the minimum temperature to 460° to 490°C (B'' in fig. 7). The minimum temperature would be further increased because none of these *Gn* + *Pg* assemblages contains quartz, indicating they were undersaturated to some extent with respect to SiO_2. As indicated in figure 9, *Gn* + *Pg* + *Px* assemblages can exist to log a(SiO_2) values as low as −1.35. Reduced log a(SiO_2) to −1.0 will shift reaction 2 to higher temperature, raising the minimum temperature of *Gn* + *Pg* assemblages to 500°C or greater (invariant point B*).

The presence of garnets with compositions near Gr_{75} in many skarn samples also restricts minimum temperature to 500° to 520°C at X(CO_2) values greater than 0.05, based on the experiments of Chatterjee (1967) for the reaction:

$$\text{Ep}(\text{Ps}_{25}) + \text{Wo} + \text{Cc} = \text{Gr}_{75} + \text{CO}_2 + \text{H}_2\text{O} \quad (3)$$

The common occurrence of garnet-bearing assemblages with garnet compositions near Gr_{75} suggests that minimum temperatures of 490° to 520°C are probably applicable to much of the inner four skarn zones.

Maximum temperatures in the skarns are limited to 565° to 600°C by the upper temperature stability of iron-bearing epidote (Chatterjee, 1967), the occurrence of garnet plus quartz, and by the maximum temperatures of prior contact metamorphism (~ 600°C). The rare occurrences (three samples) of garnet + quartz provide a maximum temperature limit from the reaction (fig. 7):

$$\text{Gr} + \text{Qz} = \text{An} + 2\ \text{Wo} \quad (4)$$

The position of this endmember reaction, corrected for the effects of measured andradite and albite component solid solutions ($Gr_{75\text{-}90}$; $An_{75\text{-}85}$), indicates a maximum temperature for the *Gn* + *Qz* assemblages of 565° to 585°C.

Limits to minimum temperature in the outer, garnet-absent zone (E) are potentially well constrained by the occurrence of the assemblages *Px* + *Sp* + *Cc* and *Fo* + *Px* + *Cc* ± *Sp* (rare). However, equilibria defining minimum temperature for these assemblages cannot at present be precisely located, because these involve clintonite and chlorite, whose thermodynamic parameters are not precisely known. Our calculations and those of Rice (1979) approximately locate the definitive equilibria (fig. 8,

0.6, and a(clinochlore) = 0.45, based on data from tables 3 and 5. Methods of these calculations are discussed in the appendix. Letters (A) through (E) and the shaded bars directly below the T-X(CO_2) diagram designate X(CO_2) limits for the five main skarn zones in the Massive skarns. These limits are defined at 525°C by the phase equilibria in this figure. Where the bars are dashed, the X(CO_2) limits either have been defined by calculated, approximate equilibria (lower limit, zone E) or are not always applicable to that zone, because the definitive mineral assemblage is not always present. For example, calcite is not often found in zones A and B, and therefore the lower limits to X(CO_2) are not often limited to greater than 0.02 by reaction 6. For those areas lacking calcite, the lower limit to X(CO_2) is 0.00.

see reactions 9, 26, and 27) which limit minimum temperature in the outer zone of the skarn to greater than 500° to 550°C. These temperature limits are consistent with an occurrence of *Px* + *Fo* + *Cc* (sample E10-43) in one sample of skarn collected almost 100 m from the *exposed* igneous contact.

The petrologic evidence from stage I assemblages indicates skarn formation occurred within a narrow temperature range of 490° to 565°C for both inner and outer zones of the skarns. In the discussion to follow, stage I of skarn development will be modeled as an isothermal process at T = 525°C. Thermal gradients within these small skarns are likely to be minimal (D. C. Chapman, personal commun.) because of the thermal effects from passage of the large quantities of high-temperature fluid necessary for skarn formation (Taylor and O'Neil, 1977; Bowman, ms; Brown, ms).

An upper limit to the temperature during stage II of skarn formation is provided by the assemblage *Amp* + *Ep* + *Cc* + *Qz* (fig. 7). A maximum temperature of ~ 450° to 470°C is indicated in figure 7 by the cross-over of reaction (1) and the reaction:

$$\mathrm{Tr} + 3\ \mathrm{Cc} + 2\ \mathrm{Qz} = 5\ \mathrm{Di} + 3\ \mathrm{CO_2} + \mathrm{H_2O} \qquad (5)$$

corrected for measured solid solutions in amphibole (OH–$\mathrm{Tr}_{55\text{-}65}$) and epidote ($\mathrm{Ps}_{22\text{-}28}$). Minimum temperature of skarn formation for stage II is not well constrained by the mineral assemblages.

Chemical Variables

Although at any one time temperature can be expected to remain approximately constant within the small masses of skarn, spatial fluctuations or gradients in fluid compositional parameters could easily occur. The several different mineral assemblages in the Elkhorn skarns and the wide variations in garnet and pyroxene compositions suggest variations in one or more chemical variables. Fluid composition parameters likely played important roles in skarn petrogenesis. Chemical variables such as $\mathrm{X(CO_2)}$ and $\mathrm{f(O_2)}$ often have been proposed (Burt, 1971, 1974; Nokleberg, 1973; Morgan, 1975; Kerrick, 1977; Newberry, ms) to account for skarn mineralogy and some of the observed mineralogical variations. Attempts are made in this next section to place limits to these and other compositional variables to see if the variable(s) responsible for mineralogical zonation can be identified.

The chemical variables used in these next sections are those defined thermodynamically in terms of the solid phases present and that can be calculated directly from the present thermodynamic data base for the solid phases. There is no implication of actual speciation in the skarn-forming fluid. Any other species (for example, $\mathrm{H_4SiO_4}$, $\mathrm{Si^{+4}}$, et cetera) can of course be calculated if the necessary thermodynamic data exist. As noted by Ferry and Burt (1982) and as can be readily demonstrated, equivalent topologies can be obtained using other selections of variables (for example, $\mathrm{Al^{+3}/(H^+)^3}$ and $\mathrm{H_4SiO_4}$ for $\mathrm{Al_2O_3}$ and $\mathrm{SiO_2}$). Until reliable activity-composition relations can be obtained for geologic fluids at ele-

vated P-T, the choice of any set of variables is for simple convenience and has no implication for the speciation of chemical constituents in the skarn fluid. The values calculated for the variables chosen here are not incorrect, because they differ from values calculated for other species. Of course errors in the thermochemical data base will affect the calculated values for all species utilizing that data base.

Variations in H_2O:CO_2 ratios.—The variations in mineralogy within the skarns suggest that there are not common limits to $X(CO_2)$ values applicable to the skarns as a whole, although the near-ubiquitous presence of grossular-rich garnet indicates H_2O in general far exceeded CO_2 in the skarn fluid. In fact, the sequence of mineralogical zones (table 2) suggests that both maximum and minimum limits to $X(CO_2)$ values increase outward from the igneous contact toward the marble (table 6).

The presence of *Ep* + *Px* ± *Cc* assemblages in the innermost portion of the skarn (zone A) at the intrusive contact defines limits to $X(CO_2)$ values by reaction 1 and the reaction (fig. 8):

$$\text{Di} + \text{Cc} = \text{Ak} + \text{CO}_2 \qquad (6)$$

Corrected for typical solid solutions observed in epidote and pyroxene, these reactions limit $X(CO_2)$ values between 0.02 and 0.11 at 525°C.

The common presence of *Vs* + *Gn* + *Px* ± *Cc* assemblages in the inner portions of the skarns (zone B) potentially defines a widely applicable upper limit to $X(CO_2)$ values for this zone based on the reaction (fig. 8):

$$18\ \text{Vs} + 44\ \text{CO}_2 = 5\ \text{Clt} + 26\ \text{Di} + 89\ \text{Gr} + 44\ \text{Cc} + 76\ \text{H}_2\text{O} \qquad (7)$$

Calculations of this equilibrium are hindered by the lack of precise thermodynamic data for both clintonite and vesuvianite. Limited experimental data for reactions involving clintonite and vesuvianite are available (Hoschek, 1976; Olesch and Seifert, 1976; Hochella and others, 1982) from which ΔG_f° values for these two minerals potentially can be extracted. Because the compositions of run products were not reported for these experiments and because the formula for synthetic and natural vesuvianite is uncertain (Valley and others, ms), the extracted ΔG_f° values for both clintonite and vesuvianite are approximate. Therefore reaction 7 can be located only approximately at $X(CO_2)$ of 0.09 ± 0.05 at 500° to 525°C using topological considerations, estimations of ΔS_r and ΔV_r with the modified vesuvianite formula suggested by Valley and others (ms), and the experimental results of Hochella and others (1982) on the stability of Mg–vesuvianite plus quartz.

Very H_2O-rich conditions with $X(CO_2)$ values < 0.04 are required locally by the presence of perovskite (Pv) in *Gn* + *Px* + *Cc* + *Vs* assemblages by the reaction:

$$\text{Ru} + \text{Cc} = \text{Pv} + \text{CO}_2 \qquad (8)$$

Reaction 8 has not been experimentally calibrated but was calculated from ΔG_f° data by Shedlock and Essene (1979).

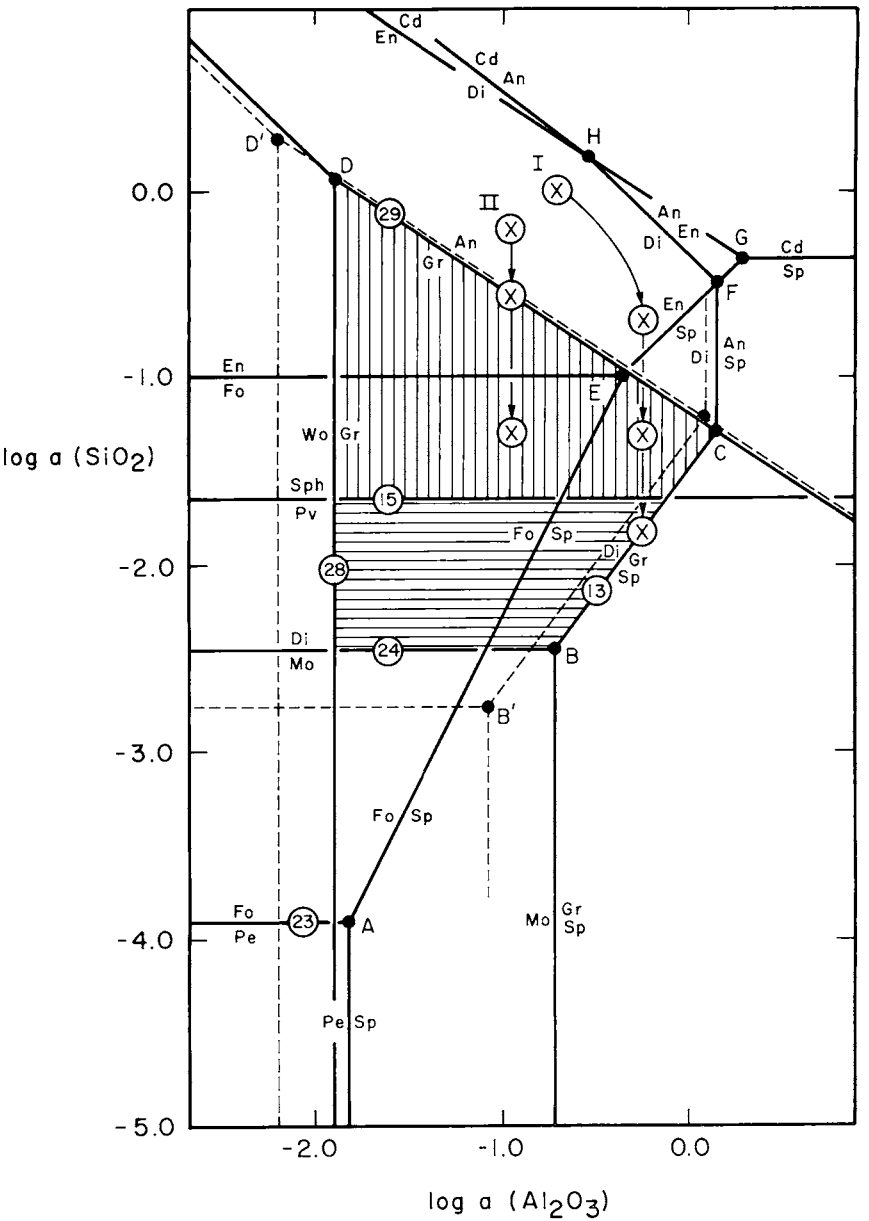

Fig. 9. Calculated $a(SiO_2)$–$a(Al_2O_3)$ diagram for equilibria relevant to skarn mineralogy at P_t = 1 kb and T = 800K. Abbreviations are: periclase (*Pe*), monticellite (*Mo*). Required thermodynamic data are listed in table 7. The vertical-striped pattern defines $a(SiO_2)$–$a(Al_2O_3)$ limits for the common skarn assemblage *Gn* + *Px* + *Sph*. Line segments B-C and C-D define activity limits for the common skarn assemblages *Gn* + *Px* + *Sp* and *Gn* + *Px* + *Pg*, respectively. The horizontally-ruled area delimits the stability of *Gn* + *Px* + *Pv* assemblages. Dashed lines denote shifts for reactions (13), (24), (28), and (29) resulting from typical mineral solid solutions within the skarns; $Gn(Gr_{75})$, $Pg(An_{80})$, $Px(Di_{75})$, and $Sp(Sp_{85})$. Paths I and II mark possible $a(SiO_2)$–$a(Al_2O_3)$ gradients that could account for observed mineral zonation sequences in the Contact skarns (table 2). Invariant point A denotes maximum possible $a(SiO_2)$–$a(Al_2O_3)$ for fluids in equilibrium with *Pe* + *Fo* + *Sp* marbles of the inner Black Butte aureole.

The absence of calcite from much of the skarn in these inner zones (A and B) indicates that $X(CO_2)$ values could have been as low as 0.00 in many areas close to the igneous contact. The low values of both maximum and minimum $X(CO_2)$ in the two inner skarn zones suggest that the CO_2 evolved during marble-to-skarn transformations (Bowman, ms) either rapidly escaped or was rapidly and effectively diluted by large masses of water.

The ubiquitous presence of grossular-rich garnet associated with *Px* and *Px* + *Cc* in the intermediate sections of the skarns (zones C and D) defines limits to $X(CO_2)$ by reactions 2 and 6. These reactions, corrected for the effect of typical garnet (Gr_{75}) and pyroxene compositions, define limits to $X(CO_2)$ (marked by the shaded bars in fig. 8) of $0.02 < X(CO_2) < 0.22$ at 525°C. These limits are generally applicable to a large fraction of skarn associated with the Black Butte stock. In detail, the actual limits of $X(CO_2)$ for any specific sample will depend on the actual garnet and pyroxene compositions. Although there is considerable range in garnet compositions ($Gr_{95\text{-}28}$) in the skarns as a whole, most (44 out of the 68 garnet analyses plotted in fig. 5) compositions are concentrated in the range $Gr_{95\text{-}65}$. Such compositions are found throughout all garnet-bearing skarn. Maximum $X(CO_2)$ values for garnet-bearing assemblages in SiO_2-undersaturated systems such as those generally encountered in the Elkhorn skarns are further restricted because reaction 2 is a function additionally of $a(SiO_2)$. A decrease in $a(SiO_2)$ to 0.10, permitted by the common *Gn* + *Px* + *Cc* assemblages (fig. 9), would reduce maximum $X(CO_2)$ to as low as 0.08 at 525°C (fig. 7).

Higher values for the minimum limit to $X(CO_2)$ are potentially available for zones C and D based on the absence of vesuvianite or if the occurrences of calcite with plagioclase represent an equilibrium assemblage. Reaction 1, corrected for typical solid solutions, provides minimum values of $X(CO_2)$ that are in the vicinity of 0.05 to 0.08 (fig. 8). Significantly higher minimum values of $X(CO_2)$ may be indicated locally by the occurrences of *Px* + *Sp* + *Cc* assemblages in zone D of the skarns, from the reaction:

$$\text{Chl} + 5\ \text{Clt} + \text{CO}_2 = 4\ \text{Di} + 11\ \text{Sp} + \text{Cc} + 9\ \text{H}_2\text{O} \qquad (9)$$

Based on a ΔG_f° value for *Clt* extracted from the experimental data of Hoschek (1976), we have calculated a preliminary location for reaction 9 at an $X(CO_2)$ value of 0.28 at 525°C and 1 kb. This is an approximate location because of the preliminary nature of Hoschek's experiments and the inprecise location of related chlorite equilibria (Bowman and Essene, 1979; Rice, 1979). Rice (1979) also calculated reaction 9 to be at an $X(CO_2)$ value of 0.35 at 525°C and 1 kb and emphasized the approximate nature of the calculation. Corrected for solid solution effects, reaction 9 provides an approximate lower limit to $X(CO_2)$ for the assemblage *Px* + *Sp* + *Cc* that is in the range of 0.20 ± 0.05 (fig. 8).

Upper limits to $X(CO_2)$ are not as well-defined for garnet-absent assemblages in the outer skarn zone (E) or the massive pyroxene at the

skarn-marble interface. At T = 525°C, diopside can exist in fluids with a wide range of $X(CO_2)$ (fig. 8). However, with reduction of log $a(SiO_2) < 1.0$, pyroxene stability in H_2O–CO_2 fluids is progressively restricted by the shift of the reaction (Kerrick, 1974):

$$Tr + 3\ Cc + 2\ Qz = 5\ Di + 3\ CO_2 + H_2O \qquad (10)$$

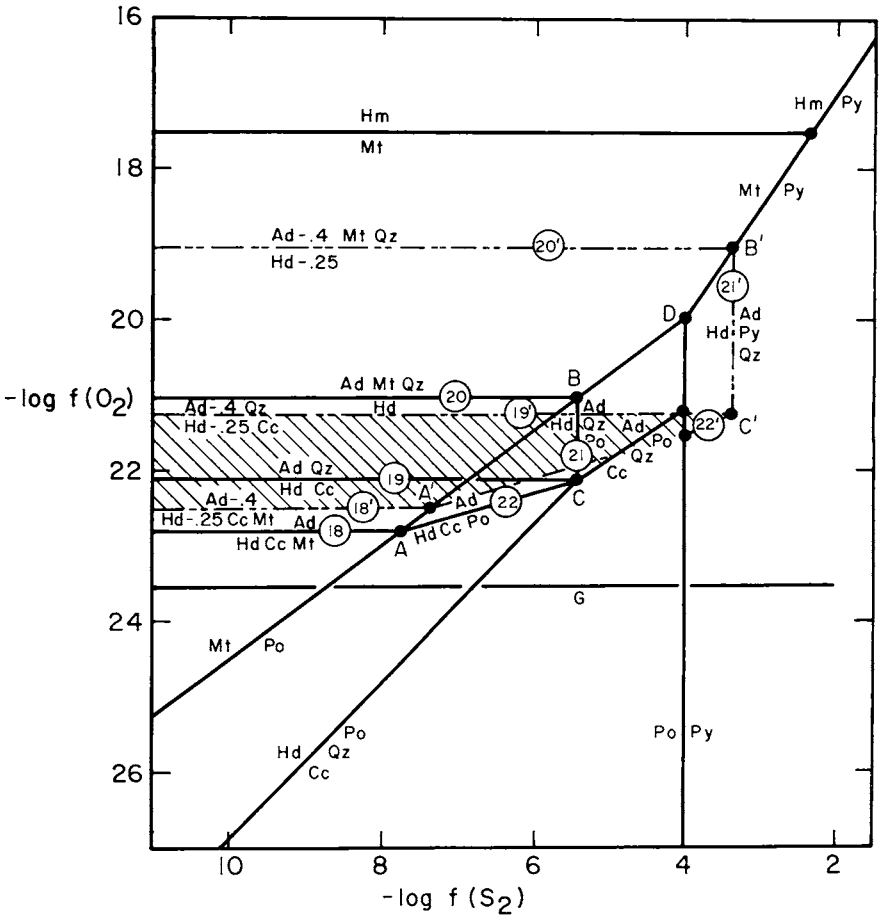

Fig. 10. Calculated $f(O_2)$–$f(S_2)$ diagram at T = 800K and P_t = 1 kb for selected silicate–sulfide–oxide–carbonate equilibria relevant to skarn mineralogy, with data from Robie, Hemingway, and Fisher (1978) and experimental data of Greenwood (1967b), Gustafson (1974), Liou (1974), and Gamble (1982). CO_2-bearing equilibria have been plotted at a constant $f(CO_2)$ = 200 bars, corresponding to $X(CO_2)$ = 0.15 at $P_t = P_f = p(CO_2) + p(H_2O)$ = 1 kb and T = 800K, given activity coefficients for H_2O and CO_2 from Burnham, Holloway, and Davis (1969) and Greenwood (1973), respectively. Abbreviations are: hematite (*Hm*), pyrrhotite (*Po*), graphite (*G*). The effects of solid solution in garnet (Ad_{40}) and pyroxene (Hd_{25}) on reactions 18 through 22 are also illustrated by the long dashed/two short dashed lines. Methods of calculating these shifts are discussed in the appendix. The ruled area outlines fugacity limits for the common skarn assemblage *Gn* + *Px* + *Cc* at Elkhorn.

to higher T and lower $X(CO_2)$. At log $a(SiO_2) = -0.7$, the maximum for *Px* + *Sp* stability (see fig. 10), reaction 10 would be shifted to $X(CO_2)$ values of less than 0.4 at 525°C. These $X(CO_2)$ values would decrease still further with any further decrease in $a(SiO_2)$. If the calcite locally present with *Px* + *Sp* assemblages has equilibrated with these phases, then this assemblage locally restricts minimum $X(CO_2)$ values in the outer zone to greater than about 0.20 ± 0.05, by reaction 9 (fig. 8).

The different $X(CO_2)$ limits defined for the five skarn zones by the various mineral assemblages are summarized in table 6. From the observed distribution of skarn mineral assemblages, it is apparent that both upper and lower limits to $X(CO_2)$ values increase outward from the igneous contact toward the marble. It is therefore possible that the actual $X(CO_2)$ values of the skarn fluids progressively increased from values between 0.00 and 0.08 near the igneous contact to values between 0.15 and 0.35 near the marble-skarn interface, if the zones formed at the same temperature. However, clear-cut petrological evidence of actual differences in $X(CO_2)$ values for adjacent zones is usually lacking because the permitted $X(CO_2)$ limits partially overlap. The overlaps arise, because solid solutions in the minerals that define the skarn zones increase the variance of the mineral assemblages.

TABLE 6

Summary of $X(CO_2)$ limits for the Massive skarn zones

Zone	Zone mineralogy	$X(CO_2)$ limits at 525°C
A	*Px* + *Ep* + *Sc* + *Cc*	0.02 to 0.11
B	*Gn* + *Px* + *Vs* + *Cc*	less than 0.08 (approximate)
C	*Gn* + *Px* + *Cc*; Absence of *Vs* and *Sp*	0.02 to 0.22
D	*Gn* + *Px* + *Pg* ± *Cc* or *Gn* + *Px* + *Sp* ± *Clt* ± *Cc*	0.05 to 0.22
E	*Px* or *Px* + *Sp* + *Cc* or *Px* + *Pg* ± *Cc*	0.15 (approximate) to 0.40

Variations in pyroxene composition also suggest variations in $X(CO_2)$ and other component activities. As noted earlier, the compositional variations in pyroxene and clintonite from *Gn* + *Px* + *Clt* + *Sp* + *Cc* and *Gn* + *Px* + *Sp* + *Cc* assemblages are far more restricted relative to the total compositional variation observed for these two minerals in the Elkhorn skarns. However, the compositions of both phases from these assemblages are not constant. If these four and five-phase assemblages are equilibrium assemblages, then the tschermaks content in pyroxene should be fixed at constant P-T-$X(CO_2)$ in the simplified chemical system CaO–MgO–Al_2O_3–SiO_2–CO_2–H_2O by the reactions:

$$(2\ Di + 5\ AlTs)_{px} + 2\ Cc = 3\ Gn + 2\ Sp + 2\ CO_2 \qquad (11)$$

$$5\ Clt + 6\ CO_2 = 11\ Di + 6\ Gn + 34\ Sp + 6\ Cc + 2\ H_2O \qquad (12)$$

In reaction 12, clintonite has the stoichiometric formula $Ca_4Mg_9Al_{14}Si_5O_{40}(OH)_8$. However, the presence of FeO and Fe_2O_3 as additional components and potential variation in $X(CO_2)$ will increase the variance of the natural system. Indeed, the pyroxenes from these two assemblages have variable tschermaks components, although the variation is significantly less in pyroxenes from the *Gn* + *Sp* + *Clt* + *Cc* assemblage (fig. 4, open circles). This small but significant variation suggests that pyroxene compositions are not strictly buffered by these skarn assemblages. Rather, the pyroxene compositions are functions additionally of the chemistry of the skarn fluids (for example, $X(CO_2)$, $a(SiO_2)$, $a(Al_2O_3)$). The SiO_2 and Al_2O_3 activities are not independent, because at constant P-T, the assemblage *Gn* + *Px* + *Sp* fixes the activity *ratio* SiO_2/Al_2O_3 by the reaction:

$$3\ Di + 4\ Al_2O_3 = Gr + 3\ Sp + 3\ SiO_2 \qquad (13)$$

Spatial variations in pyroxene composition from the assemblages *Px* + *Gn* + *Clt* + *Sp* + *Cc* and *Px* + *Gn* + *Sp* + *Cc* therefore suggest sympathetic variations in the activities of both SiO_2 and Al_2O_3 to maintain a constant activity ratio, variations in $X(CO_2)$, $f(O_2)$, or some combination of these.

Zone-boundary reactions cannot, however, result solely from variations in $X(CO_2)$. For example, reaction at the *Px* + *Pg* ± *Cc* → *Gn* + *Px* + *Pg* ± *Cc* zone boundary must involve variable $a(SiO_2)$ as well as $X(CO_2)$ in the SiO_2-undersaturated Elkhorn system even when both assemblages contain *Cc*:

$$An + 2\ Cc + SiO_2 = Gr + 2\ CO_2 \qquad (2A)$$

If calcite is absent, the conversion must involve an additional variable, the a(CaO) or $a(Ca^{++}/(H^+)^2)$ of the skarn fluids. Further, conversion of *Px* to *Gn* without participation of additional phases (rare except in Contact skarns) would not involve $X(CO_2)$ but $a(SiO_2)$, $a(Al_2O_3)$, and a(MgO) instead:

$$3\ Di + Al_2O_3 = Gr + 3\ SiO_2 + 3\ MgO \qquad (14)$$

SiO_2 and Al_2O_3 activities.—The variations in tschermaks content of pyroxenes and in hydrogarnet contents of garnets suggest that the activities of SiO_2 and Al_2O_3 in the skarn fluids may have been important variables. This is confirmed by the observation that dolomitic marble with very low content of SiO_2 and Al_2O_3 was converted to massive garnet–pyroxene skarn with no evidence of massive volume decrease which requires massive introduction of SiO_2 and Al_2O_3. Whole-rock compositional data (Bowman, ms) demonstrate transfer of significant amounts of both SiO_2 and Al_2O_3, but much less and even negligible transfer of CaO at reasonable (±20 percent) volume changes. For these reasons, the reactions in this section are written by conserving CaO rather than the usual approach of conserving Al_2O_3.

Observed skarn assemblages provide general limits for $a(SiO_2)$ and $a(Al_2O_3)$ during stage I skarn formation. Figure 9 is an appropriate activ-

ity diagram involving calc-silicate minerals at estimated skarn formation conditions of P_t = 1 kb and T = 800K (527°C). Thermodynamic data used for construction of this figure and figure 10 are compiled in table 7. The common skarn assemblage *Gn* + *Px* + *Sph* provides the following general limits (vertically ruled area, fig. 9) for stage I skarn formation, adjusted for typical solid solutions (Ad_{35}, Hd_{20}):

$$-1.65 < \log a(SiO_2) < 0.0$$

$$-1.85 < \log a(Al_2O_3) < +0.1$$

The rare assemblage *Gn* + *Px* + *Pv* provides the activity limits denoted by the horizontally ruled area (fig. 9).

Local fluctuations in both $a(SiO_2)$ and $a(Al_2O_3)$ are certainly indicated by some of the mineralogical variations observed in the skarns, if skarn formation was an isobaric, isothermal process. The occurrence of quartz-bearing, quartz-absent, and *Gn* + *Sp*-bearing assemblages in the skarn requires fluctuation in log $a(SiO_2)$ values from 0.0 to at least −1.1. The occurrence of two skarn samples that contain minor perovskite (identified with energy-dispersive electron microprobe techniques) indicates values of log $a(SiO_2)$ in these two samples below −1.6, the equilibrium log $a(SiO_2)$ value of the reaction:

$$Pv + SiO_2 = Sph \tag{15}$$

Additionally observed zonation sequences within the Contact skarn such as:

$$Pg + Px + Qz + Sph \text{ (endoskarn)} \rightarrow Pg + Px + Sph \text{ (endoskarn)} \rightarrow Gn + Px + Sph \rightarrow Gn + Px + Sp + Sph \text{ (rare) or } Px + Sp \tag{I}$$

$$Pg + Px \text{ (endoskarn)} \rightarrow Px + Pg + Gn + Sph \text{ (endoskarn)} \rightarrow Px + Gn + Sph \tag{II}$$

could be accounted for by the isothermal isobaric activity gradients labeled I and II, respectively, in figure 9. Sequence I restricts maximum log $a(Al_2O_3)$ at 527°C and 1 kb P_T to that of invariant point C: +0.1. The $a(SiO_2)$ for sequence I decreases from the quartz–diorite intrusion (log $a(SiO_2)$ = 0.0) into the massive *Gn* + *Px* + *Sp* or *Px* + *Sp* skarns with log $a(SiO_2) < -1.0$.

Variations in the tschermaks component of the skarn pyroxenes also suggest variations in the $a(SiO_2)$, if skarn formation was an isothermal, isobaric process. At constant P-T, the Al-tschermaks component dissolved in pyroxene provides, in the absence of anorthitic plagioclase, an upper limit to the $a(SiO_2)$ from the reaction and log K expression:

$$(CaAl_2SiO_6)_{Px} + SiO_2 = (CaAl_2Si_2O_8)_{Pg} \tag{16}$$

$$\log K = \Delta G^o/2.303RT + \log a_{An}^{Pg} - \log a_{AlTs}^{Px}$$

If the pyroxenes in the Elkhorn skarns formed at similar P-T, the variations in the tschermaks content of these pyroxene indicate variations

in *maximum* log $a(SiO_2)$ levels within the skarns. These maximum values will vary from as low as −2.40 for the highest measured Al-tschermaks component (42 mole percent) to values close to quartz saturation for Al-poor pyroxenes associated with garnet and plagioclase (less than 2-7 mole percent Al-tschermaks). The *Px* + *Pg* assemblages buffer, at constant P-T-An content, the log $a(SiO_2)$ to much higher values (−0.1 to −0.25) than the maximum permitted for samples with aluminous pyroxenes. The small but real variation of Al-tschermaks component (2-7 mole percent) in the pyroxenes associated with Ca–plagioclase of constant anorthite content also demonstrates variations in the $a(SiO_2)$ between different samples of this assemblage, if these formed at the same P-T. If these samples containing *Px* + *Pg* and *Px* formed at the same time as well, then the variable Al-tschermaks content of the pyroxenes demonstrates spatial gradients in $a(SiO_2)$ within the skarns.

Variations in the hydrogarnet content of garnets also suggest gradients in chemical variables. For example, garnets with maximum hydrogarnet content (7-13 mole percent) are from the mineralogically zoned, SiO_2-poor Nodule skarns (sample E1-35a) or from *Gn* + *Px* + *Sp* assemblages with log $a(SiO_2) < -1.3$ (fig. 9). In contrast, two analyzed garnets with essentially no hydrogarnet component are from quartz-bearing assemblages containing pyroxene with negligible tschermaks (samples E2-56a, E2-50), with log $a(SiO_2) = 0.0$. These data suggest that the hydrogarnet content of garnet is not only a function of water pressure and temperature but is additionally a function of the $a(SiO_2)$:

$$Ca_3Al_2Si_3O_{12} + 6\ H_2O = 3\ SiO_2 + Ca_3Al_2(OH)_{12}\ , \qquad (17)$$

and variation in the hydrogarnet content of skarn garnets suggests fluctuation in the activity of SiO_2 or fugacity of H_2O in the metasomatic fluids. At maximum possible $a(SiO_2) = 1.0$, free SiO_2 as quartz will be present, and the hydrogarnet content will be a minimum (perhaps zero) for any given $f(H_2O)$ and T. Based on the garnet compositions at Elkhorn, garnets should contain negligible amounts of hydrogarnet (less than 1 percent) for $a(SiO_2) = 1.0$ at the estimated conditions for formation of the Elkhorn skarns, $P_T = P_f = 1$ kb and T = 490° to 560°C. These natural data are in accord with the experimental results of Huckenholz and Fehr (1982) on the extent of hydrograndite solution in grandite garnets.

The entire zonation sequence of the Massive skarns cannot, however, result solely from variations in $a(SiO_2)$ and $a(Al_2O_3)$. The topology of figure 9 indicates that no simple $a(SiO_2)$–$a(Al_2O_3)$ gradient resulting from the progressive interaction of skarn fluid (initially saturated with *Px* + *Pg* + *Qz*) with marble (*Pe* + *Sp* + *Fo*) completely produces the observed zonation in Massive skarns.

Fugacities of O_2 and S_2.—General $f(O_2)$-$f(S_2)$ limits during skarn formation of the stage I skarns are provided by application of silicate–sulfide–oxide–carbonate equilibria shown in figure 10 to observed skarn assemblages. Decarbonation equilibria have been plotted at a constant $f(CO_2) = 200$ bars, a value consistent with the presence of garnet ($0.60 < X_{Gr} < 0.85$) and absence of epidote.

Application of reactions 18, 19, and 20 (fig. 10), corrected for the effects of typical garnet and pyroxene solid solution ($X_{Hd} = 0.25$, $X_{Ad} = 0.40$), to the common skarn assemblages *Gn* + *Px* + *Cc*, *Gn* + *Px* and *Gn* + *Px* + *Mt* + *Cc* (uncommon) provides the following $f(O_2)$ limits respectively:

$$-22.7 < \log f(O_2) < -21.2 \text{ (diagonally ruled area of fig. 10)}$$

$$-22.7 < \log f(O_2) < -19.0$$

$$-22.7 < \log f(O_2) < -22.5$$

These limits to $f(O_2)$, the absence of *Po*, and the scarcity of *Py* limit maximum values of log $f(S_2)$ to values below reactions 21′ (less than −3.3 at log $f(O_2) = -21.2$) and 22′ (fig. 10). Lower limits to log $f(S_2)$ values are not available from observed mineral assemblages. Rare *Gn* + *Px* + *Cc* + *Py* assemblages locally limit log $f(S_2)$ to between −4.0 (the lower limit to Py stability) and −3.3 (intersection of the reactions 19′, 21′, and 22′) for typical garnet and pyroxene compositions. These limits to log $f(S_2)$ have questionable applicability to the entire skarn, however.

It should be emphasized that the actual limits to log $f(O_2)$ for any given sample will depend on both the actual value of $f(CO_2)$ and the specific compositions of garnet and pyroxene for that sample. Variation in $X(CO_2)$ within the skarns will of course produce appropriate variations in these $f(O_2)$ limits. For example at $f(CO_2) = 100$ bars (corresponding to a value of $X(CO_2) \cong 0.08$, defined by the absence of Ep in Pg (An_{80}) + *Gn* (Gr_{75}) + *Cc* skarns), $f(O_2)$ values for reaction 18 and the graphite line would decrease by just less than half a log-unit. Because the mineral assemblages typically limit $f(CO_2)$ values to no closer than 100 to 300 bars, corresponding to a range of $X(CO_2)$ values between 0.08 and 0.22, log $f(O_2)$ limits for the common skarn assemblage *Gn* + *Px* + *Cc* could be expanded by about one log unit on either side to more realistic limits of $-23.7 < \log f(O_2) < -20.2$.

DISCUSSION

Development of contact skarn at Elkhorn primarily involved massive replacement of dolomitic marble by a variety of three-phase assemblages but principally *Gn* + *Px* + *Cc*. These varied mineralogies are imperfectly zoned with respect to the igneous contact. Subsequent replacement of these assemblages, principally by hydrous silicates and sulfides, occurred locally and to a limited extent.

Skarn is more extensively developed on the upper sides and top of the Black Butte stock (fig. 2; Klepper, Weeks, and Ruppel, 1957). Extensive lateral growth of skarn was restricted to the upper sides of the intrusion, along fractures, beneath intrusive salients within the marble wallrock, or immediately below impermeable shale units (fig. 2). The distribution of skarn suggests dominantly upward and outward flow of the skarn fluids from the intrusion and intrusive contact. Fluid flow was generally restricted to within a meter of the igneous contact at lower

levels as evidenced by the generally restricted development of skarns at these levels.

Application of phase equilibria to observed contact metamorphic and skarn assemblages indicates that the initial stage of skarn development (I) occurred at $P_T = 1.0 \pm 0.3$ kb and $T = 525 \pm 35°C$. The mutual consistency of temperature limits inferred from various mineral assemblages by the application of appropriate phase equilibria supports a reasonable approach to equilibrium by the skarn assemblages and the near-isothermal ($\pm$ 25°C) nature of early (stage I) skarn development. The hydration and carbonation reactions characterizing stage II occurred at lower temperature ($T \leqslant 450°C$) in a water-rich fluid, with $X(CO_2)$ values between 0.05 and 0.15. Close definition of P-T conditions for stages III and IV is not possible, but temperatures less than 350° to 400°C are likely from the occurrence of the assemblages Chl + Cc + Qz (stage III) and chlorite or serpentine (stage IV).

General limits to some chemical variables for stage I are available from the relatively common occurrence of appropriate limiting assemblages:

$$0.04 < X(CO_2) < 0.30$$

$$-22.7 < \log f(O_2) < -19.0$$

$$\log f(S_2) < -3.3$$

$$-1.65 < \log a(SiO_2) < 0.0$$

$$-1.85 < \log a(Al_2O_3) < +0.1$$

Because of the typically high variance of skarn assemblages, it is not possible to place close limits on all these variables in any one mineralogical zone, nor is it possible to document clearly which variables are responsible for specific zone boundary reactions. These data do indicate that the initial stage of skarn formation at Elkhorn was characterized generally by water-rich and SiO_2-undersaturated fluids and by relatively low $f(O_2)$ values comparable to those defined for tungsten skarns (Brown, ms; Einaudi, Meinert, and Newberry, 1981).

Recent studies (Takenouchi and Kennedy, 1965; Gehrig, ms; Jacobs and Kerrick, 1981; Bowers and Helgeson, 1983a, b) indicate that the addition of NaCl can significantly increase the $a_{CO_2}^{fluid}$ in CO_2-bearing aqueous fluids. As a consequence of this increase, CO_2-bearing phase equilibria used to define limits to $X(CO_2)$ for skarn petrogenesis at Elkhorn (for example, the type $A = B + CO_2$) will be shifted to lower $X(CO_2)$ values, at a given temperature, on an isobaric T-$X(CO_2)$ diagram. The effect is greatest in fluids with low $X(CO_2)$ and increases with increasing concentration of NaCl (Bowers and Helgeson, 1983b). Therefore the limits cited above for skarn petrogenesis should be regarded as maximum values. The extent of the decrease in $X(CO_2)$ can be estimated, given limits to the salinities of the skarn fluids. Salinities for the Elkhorn skarn fluids are likely in the range 5 to 15 wt percent NaCl equivalent. This range is based on the absence of daughter salts in the fluid inclusions

found in stage I minerals, on a few preliminary freezing measurements (J. R. Bowman, unpub. data), and by analogy to skarns formed under similar P-T conditions and with similar silicate mineralogy such as the CanTung, Northwest Territories skarn. Salinities of early skarn fluids at the CanTung skarn range from 4 to 14 wt percent NaCl (Mathieson, ms). Using either the empirical results of Jacobs and Kerrick (1981) or the fugacity coefficient data of Bowers and Helgeson (1983a), the effect of 5 to 15 wt percent NaCl would be to shift equilibria such as reaction 2 to approx 15 to as much as 40 percent lower $X(CO_2)$ values in the H_2O-rich region ($0.05 < X(CO_2) < 0.25$). For example, the upper limit to $X(CO_2)$ for the stability of garnet (Gr_{70} at 525°C), defined by reaction 2, would decrease from 0.22 to at least 0.19 and possibly as low as 0.13. Clearly, the values listed above for $X(CO_2)$ limits are maximum values. However, the *relative* positions of equilibria in T-$X(CO_2)$ section and, therefore, the resulting gradient in $X(CO_2)$ that is inferred for the Elkhorn skarns will be qualitatively unaffected.

Both the extensive variation in mineralogy and variations in garnet–pyroxene compositions observed in the skarns suggest that skarn formation during stage I was characterized by significant fluctuations in the activities of several chemical variables from one location to another within the skarns. Variations in garnet–pyroxene compositions (for example, hydrogarnet and Al-tschermaks components) and several sequences of mineral zonation do indicate fluctuations in the activities of CO_2, SiO_2, Al_2O_3, and total FeO_x, if skarn formation were an equilibrium isobaric, isothermal process. The importance of these variables in skarn formation and zonation at Elkhorn is reinforced by bulk chemical evidence requiring significant transfer of these chemical components during skarn formation (Bowman, ms). Variations in $f(O_2)$ are suggested by variations in iron partitioning between garnet and pyroxene, but fluctuations only of $f(O_2)$ do not duplicate any observed mineralogical sequences in the Elkhorn skarns.

Phase equilibria applications to definitive mineral assemblages are consistent with gradients in $X(CO_2)$ values of the skarn fluids from values between 0.00 and 0.08 near the igneous contact to values between 0.15 to 0.35 at the skarn-marble interface (table 6). It should be emphasized that because $X(CO_2)$ limits for adjacent zones usually partially overlap because of solid solution effects and the underdetermined nature of the skarn assemblages, clear-cut petrologic evidence of actual differences in $X(CO_2)$ values across zone boundaries is usually lacking. Nevertheless, progressive increases in $X(CO_2)$ values away from the igneous contact are consistent with mass balance calculations (Bowman, ms) which demonstrate the evolution of significant quantities of CO_2 at the skarn-marble interface and with oxygen isotope data to be presented in part 2. Variations in $X(CO_2)$ could be maintained by variable mixing of H_2O-rich skarn fluids emanating from the intrusive contact with CO_2 evolved by early metasomatic conversion of marble to skarn. Such mixing would be reasonable, resulting from expected CO_2 migration down chemical potential and/or

density gradients from the marble-skarn interface into the skarn interior. Encroachment of inner zones formed at lower $X(CO_2)$ on outer zones formed at higher $X(CO_2)$ may well mark the progressive dispersal of early-evolved CO_2 upon continued influx of H_2O-rich fluids from the intrusive contact.

Timing relations between mineral zones are not completely clear because the available exposures of zone contacts exhibit gradational, massive replacement, and cross-cutting features. These features can be interpreted in terms either of spatial migration of a contact between two adjacent, contemporaneous zones or of an inner, later zone encroaching on a previously formed zone. The first interpretation requires simultaneous development of zones in response to spatial gradients in compositional variables. Zoning in several skarns has been interpreted in terms of contemporaneous zones and, by implication, contemporaneous gradients in the variables responsible for zoning (Kerrick, 1977; Brown, ms; Dick, ms; Newberry, 1982). We have interpreted the characteristics of the zone boundaries at Elkhorn to be consistent with near-contemporaneous development of the zones, although we recognize that the available evidence is not definitive and that our interpretation may be a simplification. Given this assumption, the observed variations in mineral assemblages (zoning) and mineral compositions are interpreted to indicate gradients in the activities of one or more compositional variables. The alternative interpretation views zoning as a response through time to changing physical-chemical conditions, in which context any differences in the limits to fluid compositional variables from zone to zone represent variations in the activities of these components over time as well as space. In such a case, temperature may be an additional variable. Although small changes in temperature would permit adjacent assemblages at a zone boundary to exist at similar $X(CO_2)$ values, large temperature changes ($\geqslant 100°C$) would be required to compensate for maximum possible differences in $X(CO_2)$ values or to negate the differences in log $a(SiO_2)$ values outlined earlier. Temperature changes in excess of 175°C would be required to compensate for the minimum difference in log $a(SiO_2)$ values between *Gn* + *Px* + *Qz* and *Gn* + *Px* + *Sp* assemblages and between pyroxenes containing the minimum and maximum Al-tschermaks component. However, large temperature changes across the skarn bodies are precluded by the assemblages *Fo* + *Px* + *Cc* and *Px* + *Sp* + *Cc* in the outer skarns which restrict temperature to greater than about 525°C (see earlier discussion on temperature limits and Rice, 1979), similar to that required in the inner skarn zones. Although small changes in temperature ($\sim 25°C$) are possible, large changes are not recorded in the skarn mineralogy and are unlikely based on heat-flow considerations (D. R. Chapman, personal commun.). Formation of the skarn zones under approximately isothermal conditions is consistent with, but does not require, the contemporaneous formation of the skarn zones.

The replacement of marble by skarn at igneous contacts along the upper sides and top of the Black Butte stock suggests that skarn forma-

tion can be considered the result of the physical-chemical interaction between marble wallrock and the Black Butte stock or fluids equilibrated with the stock. Such interaction, whether the result of influx of "magmatic" fluids or convective inflow of fluids of diverse origins which have equilibrated with the igneous mineralogy, should be expected, because the mineral assemblages in the two rock types restrict the activities of several chemical components to significantly different values.

Values of $X(CO_2)$ are no doubt higher in both marble and skarn than in the intrusion. At the marble-skarn interface, $X(CO_2)$ increases sharply from a value of less than 0.07 (Bowman and Essene, 1982), to values between 0.20 and 0.35 within the outer skarn. This abrupt increase in $X(CO_2)$ was the result of the release of significant quantities of CO_2 during the initial transformation of marble to skarn.

Significant differences in $a(SiO_2)$ also exist between marble, skarn, and intrusion. *Fo* + *Sp* + *Pe* assemblages in the marble put an upper limit to log $a(SiO_2)$ of less than −3.9, defined by the reaction:

$$2\,Pe + SiO_2 = Fo \qquad (23)$$

This value is much lower than both the minimum log $a(SiO_2)$ value of −1.60 defined by the common occurrence of sphene-bearing assemblages in the inner skarn, the value of −2.75 defined in the skarns by the ubiquitous presence of pyroxene (fig. 9) via the reaction:

$$Mo + SiO_2 = Di\ , \qquad (24)$$

and the log $a(SiO_2) = 0.0$ defined by the SiO_2-saturated nature of the quartz–diorite intrusion. However, there was no simple gradient in $a(SiO_2)$ from the marble through skarn into the intrusion, as discussed earlier. In addition, the marble-skarn boundary cannot be explained by any simple and continuous gradient of $a(SiO_2)$ and/or $a(Al_2O_3)$. Additional variables such as $X(CO_2)$, a(MgO), et cetera, must be involved in the conversion of marble to pyroxene skarn.

In contrast, the range of $f(O_2)$ inferred for the skarn overlaps both that defined for the intrusion and that of the preexisting marble. *Mt* + *Po* and *Mt* + *Py* assemblages are common within the contact metamorphosed marbles of the Black Butte aureole. At 525°C, these assemblages provide broad limits (fig. 10) of:

$$Mt + Po\text{: } \log f(O_2) < -20;\ \log f(S_2) < -4.0$$

$$Mg + Py\text{: } -20 < \log f(O_2) < -17.5;\ -4 < \log f(S_2) < -2.4$$

These two assemblages are found throughout the marble, suggesting $f(O_2)$-$f(S_2)$ values are in the vicinity of the *Mt* + *Po* + *Py* triple point:

$$\log f(O_2) = -20$$

$$\log f(S_2) = -4$$

The assemblage $Bi(Ann_{40\text{-}53})$ + *Qz* + *Mt* in the Black Butte stock, *if* equilibrated at 525°C and $P(H_2O) = P_t = 1000$ bars, would fix maximum

log $f(O_2) = -15.2$ or the maximum stability of *Mt* (fig. 10). This value was calculated by rearranging eq (6″) of Wones and Eugster (1965), utilizing the activity model of Mueller (1972) for biotite and a fugacity coefficient for H_2O from Burnham, Holloway, and Davis (1969). Alkali feldspar and magnetite solid solutions were arbitrarily ignored to calculate the maximum log $f(O_2)$ value for biotite stability. The intrusion generally does not contain *Kfs*, permitting it lower log $f(O_2)$ levels, including the range defined for the skarn and host marble. The overlapping $f(O_2)$ limits for intrusion, skarn, and marble would permit skarn formation to take place at nearly constant $f(O_2)$.

As a result of chemical interaction — direct or indirect — between the stock and marble wallrock, the Elkhorn skarns exhibit a great variety of mineral assemblages which are imperfectly zoned with respect to the igneous contact. Such zoning should be a basic aspect of skarn formation, and, indeed, many skarns exhibit some degree of zoning, including those that are mineralized sufficiently to be economic sources of metals (Einaudi, Meinert, and Newberry, 1981). For example, the tungsten (scheelite) skarns at Pine Creek, Calif. are zoned outward from the igneous contact in the sequence $Gn + Px + Qz \rightarrow Vs + Px + Gn + Wo + Cc \rightarrow$ Marble (Brown, ms; Newberry, 1982). However, the variability in observed mineral assemblages and the development of zonation at Elkhorn are unusually high, when compared to many skarns that are extensively mineralized.

The Elkhorn skarns display several other characteristics in addition to the mineralogical and zoning characteristics just discussed which, when taken in sum, are unusual with respect to many mineralized skarns. The Elkhorn skarns contain relatively low-variance mineral assemblages. Whereas most skarns are characterized at any one location or time by one- or two-phase assemblages, three-phase assemblages are the norm at Elkhorn, with four- and even five-phase assemblages observed on occasion. In this respect, the Elkhorn skarns compare better to Crestmore (Burnham, 1959) than to the mineralized skarns such as Pine Creek (Brown, ms; Newberry, 1982) or Mason Valley (Einaudi, 1977). The Elkhorn skarns are further characterized by wide ranges in the compositions of garnet and pyroxene, by the presence of apparently primary hydrous silicates, and by the generally restricted development of later, retrograde alteration. These features are consistent with extensive development of gradients or fluctuations in the activities of several compositional variables, features that are not as well recorded in skarns of higher variance and with less developed zonation.

The extensive development of gradients in compositional variables that are recorded in the Elkhorn skarns may be the result in large part to lower mass ratios of skarn fluid (W) to marble (R) replaced. Lower W/R ratios or increased interaction of skarn fluids with marble wallrock may be recorded in the mineralogy and mineral compositions of the skarns by higher values of $X(CO_2)$. The causes for relatively lower W/R ratios could be manifold. Three that could be of importance are the

comparatively great depth of skarn development (P_T = 1 kb); magma emplacement and skarn development in relatively impermeable, massive marble; and skarn replacement of dolomitic, rather than calcitic marble. Variations in the bulk composition of the rock replaced by skarn do have an often profound effect on the mineralogy and zoning developed in a skarn. For instance, skarn replacing calcitic marble often has an outer wollastonite zone, whereas skarn replacing dolomitic marble is often characterized by an outer pyroxene zone. There will be differences in the amount of CO_2 released from the two types of marble as well. For each cm^3 or gram replaced, dolomitic marble will release 15 and 18 percent, respectively, more moles of CO_2 than calcitic marble. Thus for a given W/R mass ratio, skarn replacement of dolomitic as opposed to calcitic marble will likely result in higher $X(CO_2)$, other factors being equal.

The Elkhorn skarns, in comparison with many other skarns, are characterized by zonation of comparatively low-variance assemblages which have provided some evidence for gradients or fluctuations in the activities of several chemical variables. Nonetheless they result from fluid-marble interaction in a chemically open system and are still high-variance systems. Because of their high variance, petrologic studies alone have not been able to define closely chemical variables in all zones, nor have they been able to document clearly which variables are responsible for the mineralogical zonation or specific zone-boundary reactions. Many zone-boundary reactions are likely functions of several chemical variables rather than a single variable. Significantly, the complete zonation sequence of the Massive skarn (stage I), including the marble-skarn interface, cannot be explained by any simple continuous activity gradient involving only one of the chemical variables. Rather, variations in the activities of more than one chemical variable on several scales appear to be the rule rather than the exception in skarn formation at Elkhorn. Additional techniques for defining temperature limits and fluid composition parameters clearly must be applied to geologically well characterized skarns to define more precisely their environments of formation. In particular, stable isotope and fluid inclusion techniques, as well as theoretical modeling of water-rock interaction in the skarn environment, are approaches that offer good promise. Certainly the hypothesis of lower W/R ratios and the existence of $X(CO_2)$ gradients need to be tested with stable-isotope techniques to see if these are viable mechanisms for skarn formation at Elkhorn.

Appendix I

Chemical analyses.—Silicate chemical analyses were performed by wave length-dispersive electron microprobe analysis techniques using standard operating procedures and natural well-analyzed standards (Bohlen and Essene, 1977; Bowman, ms). Spectrometer data were reduced using the Fortran program EMPADR VII written by Rucklidge and Gasparrini (1969). Formula reduction procedures used are described in Shedlock and Essene (1979 — pyroxenes) and Bowman (ms — garnet and hydrous phases). Because of the usual SiO_2-undersaturated skarn bulk compositions, garnets cannot be assumed to have three Si atoms per twelve oxygen atoms. For this reason, cation proportions have been first normalized to five VI and VIII cations, and no Al was placed in the IV site. In this manner, a hydrogarnet component was calculated based

on tetrahedral (IV) site Si deficiency. All iron was assumed ferric except that necessary to balance Ti^{+4} by the relationship: $2\ R^{+3} = Fe^{+2} + Ti^{+4}$.

Thermodynamic calculations.—Experimental T-X(CO_2) phase equilibria applicable to the skarn systems are from Newton (1966), Greenwood (1967a, b), Boettcher (1970), Gordon and Greenwood (1971), Johannes and Orville (1972), Liou (1973, 1974). These equilibria have been extrapolated where necessary to 1 kb, the estimated load pressure of skarn formation, using a mixed-volatile equilibrium calculation program created by V. Wall and E. J. Essene (unpub.). This program calculates values of ΔG_r as a function of P-T-X(CO_2) from the standard relationships (Slaughter, Kerrick, and Wall, 1975). The necessary thermochemical data for solid phases utilized in these calculations are from Robie, Hemingway, and Fisher (1978) except as noted in table 7. The free energy for andradite is an average of the values extracted from the experimental data of Gustafson (1974), Liou (1974), and Gamble (1982), all of which agree closely. The result, if computed at 298K, agrees well with the estimate of W. P. Nash (1974, personal commun.) but is more negative by about 20 K joules than the value based on the experiments of Taylor and Liou (1978). Using the value for andradite in table 7, the free energy value for hedenbergite was extracted from other experimental data of Gustafson (1974). Changes in the free energy value for andradite will modify somewhat the equilibrium log $f(O_2)$ position of any single equilibrium involving andradite. As the free energy values for andradite and hedenbergite are interconnected, the relative positions of andradite and hedenbergite-bearing equilibria will be affected to a lesser degree. Thermodynamic data for H_2O and CO_2 are from Burnham, Holloway, and Davis (1969), Price (1955), and Victor J. Wall (unpub.).

Equilibria involving clintonite were calculated using a $\Delta G_f°$ value for clintonite (table 7) extracted from the experimental data of Hoschek (1976), the only experimental

TABLE 7

Sources of thermodynamic data for the calculated phase equilibria of this study

Phase	Formula	Abbreviation	$\Delta G_f°$ (800K, 1 bar) (Kj/mole)	Reference	V°(298K) (cm^3)	Ref.
akermanite	$Ca_2MgSi_2O_7$	Ak	−3349.260	(1)	92.81	(1)
andradite	$Ca_3Fe_2Si_3O_{12}$	Ad	−4928.798	(2)	131.65	(8)
anhydrite	$CaSO_4$	Ah	−1133.629	(1)	45.94	(1)
anorthite	$CaAl_2Si_2O_8$	An	−3628.086	(1)	100.79	(1)
clinochlore	$Mg_5Al_2Si_3O_{10}(OH)_8$	Chl	−8237.878	(3)	211.40	(9)
clintonite	$Ca_4Mg_9Al_{11}Si_5O_{10}(OH)_8$	Clt	−6199.898	(4)	139.06	(9)
cordierite	$Mg_2Al_4Si_5O_{18}$	Cd	−7792.357	(1)	233.22	(1)
diopside	$CaMgSi_2O_6$	Di	−2745.390	(1)	66.09	(1)
clinoenstatite	$MgSiO_3$	En	−1314.755	(1)	31.47	(1)
forsterite	Mg_2SiO_4	Fo	−1851.575	(1)	43.79	(1)
grossular	$Ca_3Al_2Si_3O_{12}$	Gr	−5681.625	(11)	125.30	(1)
hedenbergite	$CaFeSi_2O_6$	Hd	−2430.114	(2)	67.88	(10)
hematite	Fe_2O_3	Hm	−610.777	(1)	30.27	(1)
magnetite	Fe_3O_4	Mg	−849.125	(1)	44.52	(1)
monticellite	$CaMgSiO_4$	Mo	−1950.150	(5)	51.36	(8)
periclase	MgO	Pc	−515.157	(1)	11.25	(1)
perovskite	$CaTiO_3$	Pv	−1435.573	(1)	33.63	(1)
pyrite	FeS_2	Py	−140.641	(1)	23.94	(1)
pyrrhotite	$Fe_{1-x}S$	Po	−100.767	(6)	17.62	(8)
quartz	SiO_2	Qz	−765.287	(1)	22.69	(1)
sphene	$CaTiSiO_5$	Sph	−2225.750	(7)	55.65	(8)
spinel	$MgAl_2O_4$	Sp	−1963.991	(1)	39.71	(1)
wollastonite	$CaSiO_3$	Wo	−1407.954	(1)	39.93	(1)

References: (1) Robie, Hemingway, and Fisher (1978); (2) calculated from Gustafson (1974), Liou (1974), and Gamble (1982); (3) Chernosky (1974); (4) calculated from Chernosky (1974) and Hoschek (1976); (5) Valley and Essene (1979); (6) Helgeson and others (1978); (7) calculated from Hunt and Kerrick (1977); (8) Robie, Bethke, and Beardsley (1967); (9) calculated from Robie, Bethke, and Beardsley (1967); (10) Lindsley, Munoz, and Finger (1968); (11) Westrum, Essene, and Perkins (1979) and Robie, Hemingway, and Fisher (1978).

reversal data currently available for clintonite. As noted by Rice (1979), the resultant thermochemical data will be approximate because of the relatively wide reversal brackets of the Hoschek experiments and the absence of precise information on the compositions of the experimental run products. Equilibria involving vesuvianite (reaction 7) were calculated from the topological constraints that result from combination of existing topologies in the system CaO–Al_2O_3–SiO_2–H_2O–CO_2 (Gordon and Greenwood, 1971) with the experimental data of Hochella and others (1982) and from the entropy estimates for vesuvianite of Valley and others (ms). These calculations are also approximate. Equilibria in terms of $f(O_2)$–$f(S_2)$ and $a(SiO_2)$–$a(Al_2O_3)$ were based on available experimental and thermochemical data (Holland, 1959, 1965; Liou, 1973, 1974; Gustafson, 1974; Robie, Hemingway, and Fisher, 1978; Taylor and Liou, 1978; Gamble, 1982).

Solid solution effects on phase equilibria.—The effects of solid solution on the P-T-component activity positions of phase equilibria were calculated utilizing either of the two relations:

$$\Delta S_r dT = d\,\Delta G_r = RT\,d\ln K$$

or:

$$\ln K = \ln K - \ln K^0 = \frac{\Delta Hr^0}{R}\left(\frac{1}{T} - \frac{1}{T^0}\right)$$

In the latter formulation, the superscript zero refers to the pure endmember system. The temperature T to which a reaction is shifted due to solid solutions can be calculated if ΔH_R, ln K, and ln K^0 are known or can be calculated. For equilibria portrayed at constant temperature, the appropriate activity terms for the solid solution phases were incorporated into the equilibrium constant. Activities were calculated with activity coefficient data where available or by assuming an *ideal ionic* solution model, neglecting site fractions involved in coupled substitution, and assuming complete disorder (Kerrick and Darken, 1975), except in the case of Fe–Al in epidote:

garnet	a_{Gr}^{Gn} calculated from Huckenholz, Lindhuber, and Fehr (1981)
pyroxene	a_{Di}^{Px}, a_{Hd}^{Px} from Froese and Gordon (1974)
plagioclase	a_{An}^{Pg} from Windom and Boettcher (1976)
epidote	$a_{Czo}^{Ep} = (X_{Al})\,(X_{Al})^2\,(X_{OH})$
amphibole	$a_{OH\text{-}Tr}^{Amp} = (1\text{-}X_{Na,K})\,(X_{Ca})^2\,(X_{Mg})^5\,(X_{OH})^2$
clintonite	$a_{Clt}^{Ca\text{-}mica} = (X_{Ca})^4\,(X_{Mg})^6\,(X_{OH})^2$
chlorite	$a_{clinochlore}^{Chl} = (X_{Mg})^5\,(X_{OH})^8$
spinel	$a_{MgAl_2O_4}^{spinel} = (X_{Mg})\,(X_{Al})^2$

In most cases, the equilibrium positions of reactions do not depend significantly on activity models or deviations from ideality, for the observed compositional ranges of the minerals, and for the inferred P-T conditions of skarn formation.

References

Boettcher, A. L., 1970, The system CaO–Al_2O_3–SiO_2–H_2O at high pressure and temperature: Jour. Petrology, v. 11, p. 337-370.

Bohlen, S. R., and Essene, E. J., 1977, Feldspar and oxide thermometry of granulites in the Adirondack Highlands: Contr. Mineralogy Petrology, v. 62, p. 153-169.

Bowers, T. S., and Helgeson, H. C., 1983a, Calculation of the thermodynamic and geochemical consequences of nonideal mixing in the system H_2O–CO_2–NaCl on phase relations in geologic systems: Equation of state for H_2O–CO_2–NaCl fluids at high pressures and temperatures: Geochim. et Cosmochim. Acta, v. 47, p. 1247-1275.

———— 1983b, Calculation of the thermodynamic and geochemical consequences of nonideal mixing in the system H_2O–CO_2–NaCl on phase relations in geologic systems: metamorphic equilibria at high pressures and temperatures: Am. Mineralogist, v. 68, p. 1059-1075.

Bowman, J. R., ms, 1978, Contact metamorphism, skarn formation, and origin of C–O–H skarn fluids in the Black Butte aureole, Elkhorn, Montana: Ph.D. thesis, Univ. Michigan, Ann Arbor, Mich., 462 p.

Bowman, J. R., and Essene, E. J., 1979, Clintonite-bearing assemblages in contact skarns, Elkhorn, Montana [abs.]: Am. Geophys. Union, EOS Trans., v. 60, p. 422.

———— 1982, P-T-X(CO_2) conditions of contact metamorphism in the Black Butte aureole, Elkhorn, Montana: Am. Jour. Sci., v. 282, p. 311-340.

Brown, P. E., ms, 1980, A petrologic and stable isotopic study of skarn formation and mineralization at the Pine Creek, California tungsten mine: Ph.D. thesis, Univ. Michigan, Ann Arbor, Mich., 240 p.

Burnham, C. W., 1959, Contact metamorphism of magnesian limestones at Crestmore, California: Geol. Soc. America Bull., v. 70, p. 879-920.

Burnham, C. W., Holloway, J. R., and Davis, N. F., 1969, Thermodynamic properties of water to 1000° and 10,000 bars: Geol. Soc. America Spec. Paper 132, 96 p.

Burt, D. M., 1971, Some phase equilibria in the system Ca–Fe–Si–C–O: Carnegie Inst. Washington Year Book 70, p. 178-184.

———— 1974, Metasomatic zoning in Ca–Fe–Si exoskarns, *in* Hofmann, A. W., Giletti, B. J., Yoder, Jr., H. S., and Yund, R. A., eds., Geochemical Transport and Kinetics: Carnegie Inst. Washington Pub. 634, p. 287-293.

Chatterjee, N. D., 1967, Experiments on the phase transition calcite + wollastonite + epidote = grossular–andradite$_{ss}$ + CO_2 + H_2O: Contr. Mineralogy Petrology, v. 14, p. 114-122.

Chernosky, J. V., Jr., 1974, The upper stability of clinochlore at low pressure and the free energy of formation of Mg–cordierite: Am. Mineralogist, v. 59, p. 496-507.

Collins, B. I., 1977, Formation of scheelite-bearing and scheelite-barren skarns at Lost Creek, Pioneer Mountains, Montana: Econ. Geology, v. 72, p. 1505-1523.

Cook, S. J., ms, 1982, The physical-chemical conditions of contact skarn formation at Alta, Utah: M.S. thesis, Univ. Utah, Salt Lake City, Utah, 169 p.

Dick, L. A., ms, 1980, A comparative study of the geology, mineralogy, and conditions of formation of contact metasomatic mineral deposits in the NE Canadian Cordillera- Ph.D. thesis, Queen's Univ., Kingston, Ontario, 473 p.

Einaudi, M. T., 1977, Petrogenesis of the copper-bearing skarn at the Mason Valley Mine, Yerington District, Nevada: Econ. Geology, v. 72, p. 709-795.

Einaudi, M. T., and Burt, D. M., eds., 1982, A Special Issue Devoted to Skarn Deposits: Econ. Geology, v. 77, no. 4, p. 745-1052.

Einaudi, M. T., Meinert, L. D., and Newberry, R. J., 1981, Skarn deposits: Econ. Geology, 75th Ann. V., p. 317-391.

Ferry, J. M., and Burt, D. M., 1982, Characterization of metamorphic fluid composition through mineral equilibria, *in* Ferry, J. M., ed., Characterization of metamorphism through mineral equilibria: Mineralog. Soc. America, Reviews in Mineralogy, v. 10, p. 207-262.

Fisher, J. R., and Zen, E-an, 1971, Thermochemical calculations from hydrothermal phase equilibrium data and the free energy of H_2O: Am. Jour. Sci., v. 270, p. 297-314.

Froese, E., and Gordon, T. M., 1974, Activity coefficients of coexisting pyroxenes: Am. Mineralogist, v. 59, p. 204-205.

Gamble, R. P., 1982, An experimental study of sulfidation reactions involving andradite and hedenbergite: Econ. Geology, v. 77, p. 784-797.

Gehrig, M., ms, 1980, Phasengleichgewichte und PVT-Daten ternärer Mischungen aus wasser, Kohlendioxid und Na–triumchlorid bis 3 kbar and 550°C: Ph.D. thesis, Univ. Karlsruhe, Hochschulverlag, Freiburg.

Gordon, T. M., and Greenwood, H. J., 1971, Stability of grossularite in H_2O–CO_2 mixtures: Am. Mineralogist, v. 56, p. 1674-1688.

Greenwood, H. J., 1967a, Mineral equilibria in the system MgO–SiO_2–H_2O–CO_2, *in* Abelson, P. H., ed., Researches in Geochemistry, II: New York, John Wiley & Sons, p. 542-547.

———— 1967b, Wollastonite: stability in H_2O–CO_2 mixtures and occurrence in a contact-metamorphic aureole near Salmo, British Columbia, Canada: Am. Mineralogist, v. 52, p. 1669-1680.

———— 1973, Thermodynamic properties of gaseous mixture of H_2O and CO_2 between 450° and 800°C and 0 to 500 bars: Am. Jour. Sci., v. 273, p. 561-571.

Gustafson, W. J., 1974, Stability relations of andradite, hedenbergite, and related minerals in the system Ca–Fe–Si–O–H: Jour. Petrology, v. 15, p. 455-496.

Helgeson, H. C., Delany, J. M., Nesbitt, H. W., and Bird, D. K., 1978, Summary and critique of the thermodynamic properties of rock-forming minerals: Am. Jour. Sci., v. 278-A, p. 1-229.

Hochella, M. F., Jr., Liou, J. G., Keskinen, M. J., and Kim, H. S., 1982, Synthesis and stability relations of magnesium idocrase: Econ. Geology, v. 77, p. 798-808.

Holland, H. D., 1959, Some applications of thermochemical data to problems of ore deposits, I. Stability relations among the oxides, sulfides, sulfates, and carbonates of ore and gangue minerals: Econ. Geology, v. 54, p. 184-233.

———— 1965, Some applications of thermochemical data to problems of ore deposits, II. Mineral assemblages and the composition of ore-forming fluids: Econ. Geology, v. 60, p. 1101-1166.

Hoschek, G., 1976, Zur stabilität von clintonite im system $CaO–MgO–Al_2O_3–SiO_2–H_2O–CO_2$: Fortschr. Mineralogie, v. 54, p. 39-40.

Huckenholz, H. G., Lindhuber, W., and Fehr, K. T., 1981, Stability relationships of grossular + quartz + wollastonite + anorthite, I. The effect of andradite–grossular solid solution: Neues Jahr. Mineralogie Abh., v. 142, p. 223-247.

Huckenholz, H. G., and Fehr, K. T., 1982, Stability relationships of grossular + quartz + wollastonite + anorthite, II. The effect of grandite–hydro-grandite solid solution: Neues Jahr. Mineralogie Abh., v. 145, p. 1-33.

Hunt, J. A., and Kerrick, D. M., 1977, The stability of sphene: experimental redetermination and geological implications: Geochim. et Cosmochim. Acta, v. 41, p. 279-288.

Jacobs, G. K., and Kerrick, D. M., 1981, Devolatilization equilibria in $H_2O–CO_2$ and $H_2O–CO_2–NaCl$ fluids: an experimental and thermodynamic evaluation at elevated pressures and temperatures: Am. Mineralogist, v. 66, p. 1135-1153.

Johannes, W., and Orville, P. M., 1972, Zur stabilität der mineral paragenesen muskovit + calcit + quarz, zoisit + muskovit + quarz, anorthit + k-feldspar und anorthit + calcit: Fortschr. Mineralogie, v. 50, p. 47-60.

Kerrick, D. M., 1974, Review of metamorphic mixed-volatile equilibria: Am. Mineralogist, v. 59, p. 729-762.

———— 1977, The genesis of zoned skarns in the Sierra Nevada, California: Jour. Petrology, v. 18, p. 1-38.

Kerrick, D. M., and Darken, L. S., 1975, Statistical thermodynamic models for ideal oxide and silicate solid solutions, with applications to plagioclase: Geochim. et Cosmochim. Acta, v. 39, p. 1421-1442.

Khorzhinskii, D. S., 1959, Physiochemical Basis of the Analysis of the Paragenesis of Minerals: New York, Consultants Bur., 1970, 93 p.

Klepper, M. R., Weeks, R. A., and Ruppel, E. T., 1957, Geology of the southern Elkhorn Mountains, Jefferson and Broadwater Counties, Montana: U.S. Geol. Survey Prof. Paper 292, 82 p.

Kwak, Teunis A. P., 1978a, Mass-balance relationships and skarn-forming processes of the King Island Scheelite deposit, King Island, Tasmania, Australia: Am. Jour. Sci., v. 278, p. 943-968.

———— 1978b, The conditions of formation of the King Island scheelite contact skarn, King Island, Tasmania, Australia: Am. Jour. Sci., v. 278, p. 969-999.

Lindsley, D. H., Munoz, J. L., and Finger, L., 1968, Unit cell parameters of clinopyroxenes along the join hedenbergite–ferrosilite: Carnegie Inst. Washington Year Book, v. 67, p. 91-92.

Liou, J. G., 1973, Synthesis and stability relations of epidote, $Ca_2Al_2FeSi_3O_{12}(OH)$: Jour. Petrology, v. 14, p. 381-413.

———— 1974, Stability relations of andradite–quartz in the system Ca–Fe–Si–O–H: Am. Mineralogist, v. 59, p. 1016-1025.

Mathieson, G. A., ms, 1982, The CanTung E-zone scheelite orebody, Tungsten, N.W.T., Canada: M.S. thesis, Queen's Univ., Kingston, Ontario, 156 p.

Morgan, B. A., 1975, Mineralogy and origin of skarns in the Mount Morrison pendant, Sierra Nevada, California: Am. Jour. Sci., v. 275, p. 119-142.

Mueller, R. F., 1972, Stability of biotite: A discussion: Am. Mineralogist, v. 57, p. 300-316.

Newberry, R. J., ms, 1980, The geology and chemistry of skarn formation and tungsten deposition in the central Sierra Nevada, California: Ph.D. thesis, Stanford Univ., Stanford, Calif., 325 p.

———— 1982, Tungsten-bearing skarns of the Sierra Nevada. I. The Pine Creek Mine, California: Econ. Geology, v. 77, p. 823-844.

Newton, R. C., 1966, Some calc-silicate equilibrium relations: Am. Jour. Sci., v. 264, p. 204-222.

Nokleberg, W. J., 1973, CO_2 as a source of oxygen in the metasomatism of carbonates: Am. Jour. Sci., v. 273, p. 498-514.

Olesch, M., 1975, Synthesis and solid solubility of trioctahedral brittle micas in the system $CaO–MgO–Al_2O_3–SiO_2–H_2O$: Am. Mineralogist, v. 60, p. 188-199.

———— 1978, Obere thermische stabilität von vesuvian bis 2 kbar und vesuvian + quartz bis 5 kbar im system $CaO–MgO–Al_2O_3–SiO_2–H_2O$: Fortschr. Mineralogie, v. 56, p. 99.

Olesch, M., and Seifert, F., 1976, Stability and phase relations of tri-octahedral calcium brittle micas (clintonite group): Jour. Petrology, v. 17, p. 291-314.

Pistorius, Carl W. F. T., and Kennedy, G. C., 1960, Stability relations of grossularite and hydrogrossularite at high temperatures and pressures: Am. Jour. Sci., v. 258, p. 247-257.

Price, D., 1955, Thermodynamic functions of carbon dioxide: Indus. Eng. Chemistry, v. 47, p. 1649-1652.

Rice, J. N., 1979, Petrology of clintonite-bearing marbles in the Boulder aureole, Montana: Am. Mineralogist, v. 64, p. 519-526.

Robie, R. A., Bethke, P. M., and Beardsley, K. M., 1967, Selected x-ray crystallographic data, molar volumes, and densities of minerals and related substances: U.S. Geol. Survey Bull. 1248, 87 p.

Robie, R. A., Hemingway, B. S., and Fisher, J. R., 1978, Thermodynamic properties of minerals and related substances at 298.15 K and 1 bar (10^5 pascals) pressure and at higher temperatures: U.S. Geol. Survey Bull. 1452, 456 p.

Rucklidge, J. C., and Gasparrini, E. L., 1969, EMPADR VII: A computer program for processing microprobe analytical data: Univ. Toronto.

Shedlock, R. J., and Essene, E. J., 1979, Mineralogy and petrology of a tactite near Helena, Montana: Jour. Petrology, v. 20, p. 71-98.

Slaughter, J., Kerrick, D. M., and Wall, V. J., 1975, Experimental and thermodynamic study of equilibria in the system $CaO–MgO–SiO_2–H_2O–CO_2$: Am. Jour. Sci., v. 275, p. 445-454.

Takenouchi, S., and Kennedy, G. C., 1965, The solubility of carbon dioxide in NaCl solutions at high temperatures and pressures: Am. Jour. Sci., v. 263, p. 445-454.

Taylor, B. E., and O'Neil, J. R., 1977, Stable isotope studies of metasomatic Ca–Fe–Al–Si skarns and associated metamorphic and igneous rocks, Osgood Mountains, Nevada: Contr. Mineralogy Petrology, v. 63, p. 1-50.

Taylor, B. E., and Liou, J. G., 1978, The low-temperature stability of andradite in C–O–H fluids: Am. Mineralogist, v. 63, p. 378-393.

Valley, J. W., and Essene, E. J., 1979, Vesuvianite, akermanite, monticellite, and wollastonite equilibria and high X H_2O/CO_2 at Cascade slide, Mt. Marcy quadrangle, Adirondacks Mountains [abs.]: Am. Geophys. Union, EOS Trans., v. 60, p. 423.

Walter, L. S., 1963, Experimental studies on Bowen's decarbonation series: I: P-T univariant equilibria of the "monticellite" and "akermanite" reactions: Am. Jour. Sci., v. 251, p. 488-500.

Westrum, E., Essene, E. J., and Perkins, D., 1979, Calorimetric determination of S_T of grossularite: Contr. Mineralogy Petrology, v. 64, p. 137-148.

Windom, K. E., and Boettcher, A. L., 1976, The effect of reduced activity of anorthite on the reaction grossular + quartz = anorthite + wollastonite: a model for plagioclase in the earth's lower crust and upper mantle: Am. Mineralogist, v. 61, p. 889-896.

Wones, D. R., and Eugster, H. P., 1965, Stability of biotite: experiment, theory and application: Am. Mineralogist, v. 50, p. 1228-1272.

Zen, E-an, 1972, Gibbs free-energy, enthalpy, and entropy of ten rock-forming minerals: calculations, discrepancies, implications: Am. Mineralogist, v. 57, p. 524-553.

———— 1973, Thermodynamical parameters of minerals from oxygen-buffered hydrothermal equilibrium data: Method and application to annite and almandine: Contr. Mineralogy Petrology, v. 62, p. 153-169.

Zharikov, V. A., Shmulovich, K. I., and Bulator, V. K., 1977, Experimental studies in the system $CaO–MgO–Al_2O_3–SiO_2–H_2O$ and conditions of high-temperature metamorphism: Tectonophysics, v. 43, p. 145-162.